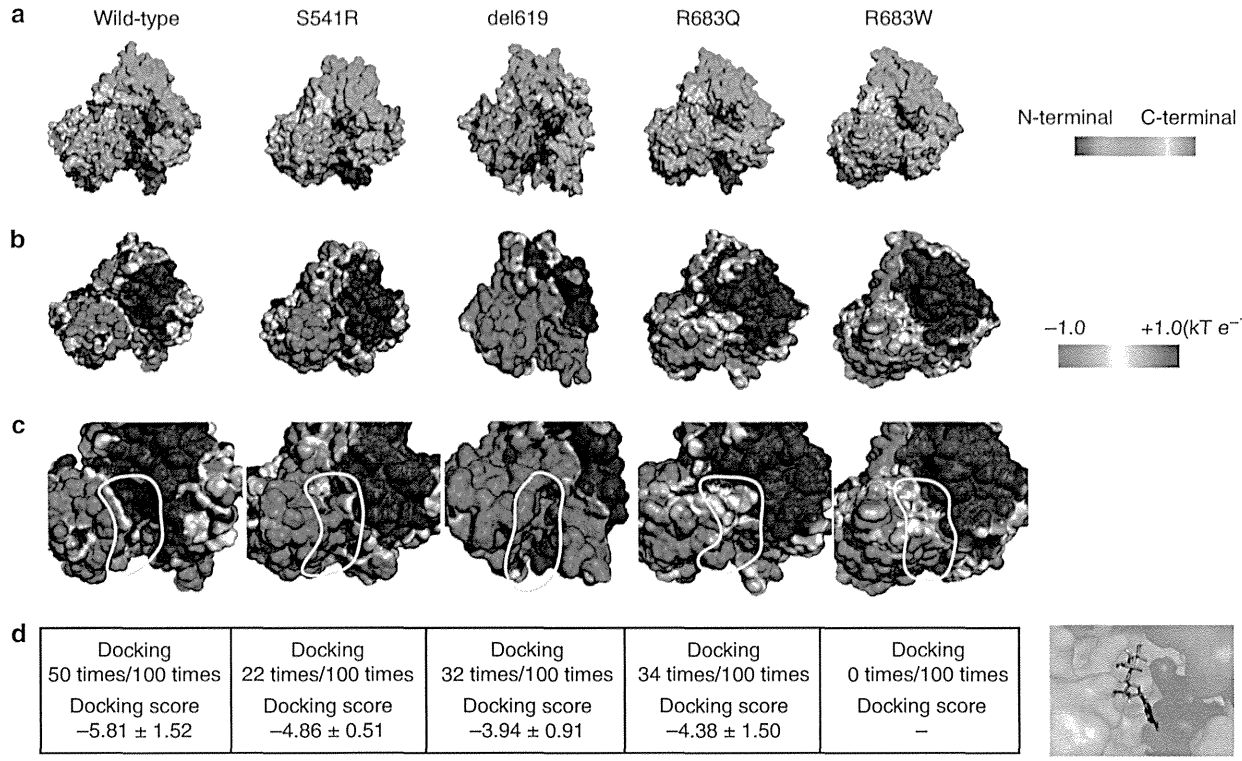

Figure 1. Comparison of three dimensional (3D) structures and electrostatic surface potentials of the XPD protein *in silico* among wild type and mutants. (**a**) 3D structures of wild-type and mutant XPD proteins (from the N terminus to the C terminus, blue to red). (**b**) Electrostatic surface potentials of XPD proteins (from negative potentials to positive potentials, red to blue). (**c**) Magnification of electrostatic surface potentials of XPD proteins at the ATP-binding site (enclosed by yellow). (**d**) Results of docking simulation of ATP and XPD proteins. The right panel shows that ATP binds to XPD protein in a previously reported site and orientation. A lower docking score indicates a more energetically stable state.

affinity than does the former. Also, in our *in silico* analysis of human XPD, the R683Q mutant has an ATP-docking ability that is weaker compared with the wild type, whereas the R683W is not capable of ATP docking. Because helicases couple the energy of ATP hydrolysis to the unwinding of DNA, these data may explain the difference in clinical severity between patients harboring R683W and those harboring R683Q. Similar to R683Q, ATP-docking ability of S541R and del619 may explain why XPD patients with these mutations experience milder symptoms.

The Medical Ethics Committee of Kobe University approved this work, which was conducted in accordance with the Declaration of Helsinki Principles. Written informed consent was obtained from all patients for participation in this study.

CONFLICT OF INTEREST

The authors state no conflict of interest.

ACKNOWLEDGMENTS

We thank Shinichi Moriwaki in the Department of Dermatology, Osaka Medical College, Takatsuki, Japan for giving us vectors for the host-cell reactivation assay. We also thank Chihiro Honda, Masamitu Ichihashi, Kaoru Tsujioka, and Ken Igawa for introducing the XP patients to us and all the patients and families who contributed to this study. We are deeply indebted to Yoko Nakagawa and Kenji Miura for their excellent technical assistance. This study was supported by Health and Labour Sciences Research Grants, Research on Intractable Diseases (CN).

Eiji Nakano[1,3], Ryusuke Ono[1,3], Taro Masaki[1], Seiji Takeuchi[1], Yutaka Takaoka[2], Eiichi Maeda[2] and Chikako Nishigori[1]

[1]Division of Dermatology, Department of Internal Related, Graduate School of Medicine, Kobe University, Kobe, Japan and [2]Division of Medical Informatics and Bioinformatics, Graduate School of Medicine, Kobe University, Kobe, Japan
E-mail: chikako@med.kobe-u.ac.jp

SUPPLEMENTARY MATERIAL

Supplementary material is linked to the online version of the paper at http://www.nature.com/jid

REFERENCES

Boyle J, Ueda T, Oh KS *et al.* (2008) Persistence of repair proteins at unrepaired DNA damage distinguishes diseases with ERCC2 (XPD) mutations: cancer-prone xeroderma pigmentosum vs. non-cancer-prone trichothiodystrophy. *Hum Mutat* 29: 1194–208

DiGiovanna JJ, Kraemer KH (2012) Shining a light on xeroderma pigmentosum. *J Invest Dermatol* 132:785–96

Emmert S, Ueda T, Zumsteg U *et al.* (2009) Strict sun protection results in minimal skin changes in a patient with xeroderma pigmentosum and a novel c.2009delG mutation in XPD (ERCC2). *Exp Dermatol* 18:64–8

Falik-Zaccai TC, Erel-Segal R, Horev L *et al.* (2012) A novel XPD mutation in a compound heterozygote; the mutation in the second allele is present in three homozygous patients with mild sun sensitivity. *Environ Mol Mutagen* 53: 505–14

Fan L, Fuss JO, Cheng QJ *et al.* (2008) XPD helicase structures and activities: insights into the cancer and aging phenotypes from XPD mutations. *Cell* 133:789–800

Kobayashi T, Kuraoka I, Saijo M *et al.* (1997) Mutations in the XPD gene leading to

xeroderma pigmentosum symptoms. *Hum Mutat* 9:322–31

Kobayashi T, Uchiyama M, Fukuro S *et al.* (2002) Mutations in the XPD gene in xeroderma pigmentosum group D cell strains: confirmation of genotype-phenotype correlation. *Am J Med Genet* 110:248–52

Liu H, Rudolf J, Johnson KA *et al.* (2008) Structure of the DNA repair helicase XPD. *Cell* 133: 801–12

Takayama K, Salazar EP, Lehmann A *et al.* (1995) Defects in the DNA repair and transcription gene ERCC2 in the cancer-prone disorder xeroderma pigmentosum group D. *Cancer Res* 55:5656–63

Taylor EM, Broughton BC, Botta E *et al.* (1997) Xeroderma pigmentosum and trichothiodystrophy are associated with different mutations in the XPD (ERCC2) repair/transcription gene. *Proc Natl Acad Sci USA* 94:8658–63

Ueda T, Compe E, Catez P *et al.* (2009) Both XPD alleles contribute to the phenotype of compound heterozygote xeroderma pigmentosum patients. *J Exp Med* 206: 3031–46

Viprakasit V, Gibbons RJ, Broughton BC *et al.* (2001) Mutations in the general transcription factor TFIIH result in beta-thalassaemia in individuals with trichothiodystrophy. *Hum Mol Genet* 10:2797–802

SCIENTIFIC REPORTS

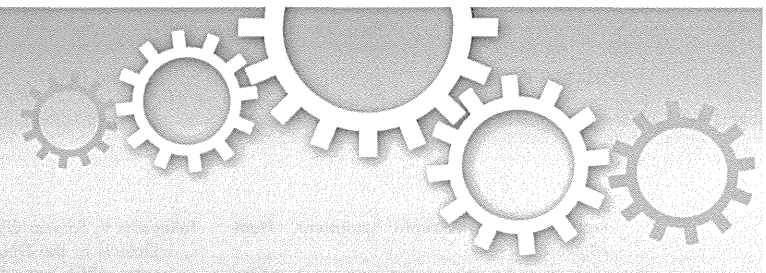

OPEN

SUBJECT AREAS:
OLIGONUCLEOTIDE PROBES
ASSAY SYSTEMS
DNA PROBES

Received
12 May 2014

Accepted
18 June 2014

Published
4 July 2014

Correspondence and requests for materials should be addressed to S.I. (iwai@chem.es.osaka-u.ac.jp)

Fluorescence detection of cellular nucleotide excision repair of damaged DNA

Tatsuya Toga[1], Isao Kuraoka[1], Shun Watanabe[1], Eiji Nakano[2], Seiji Takeuchi[2], Chikako Nishigori[2], Kaoru Sugasawa[3] & Shigenori Iwai[1]

[1]Division of Chemistry, Graduate School of Engineering Science, Osaka University, 1-3 Machikaneyama, Toyonaka, Osaka 560-8531, Japan, [2]Division of Dermatology, Graduate School of Medicine, Kobe University, 7-5-1 Kusunoki-cho, Chuo-ku, Kobe, Hyogo 650-0017, Japan, [3]Biosignal Research Center, Kobe University, 1-1 Rokkodai, Nada-ku, Kobe, Hyogo 657-8501, Japan.

To maintain genetic integrity, ultraviolet light-induced photoproducts in DNA must be removed by the nucleotide excision repair (NER) pathway, which is initiated by damage recognition and dual incisions of the lesion-containing strand. We intended to detect the dual-incision step of cellular NER, by using a fluorescent probe. A 140-base pair linear duplex containing the (6–4) photoproduct and a fluorophore–quencher pair was prepared first. However, this type of DNA was found to be degraded rapidly by nucleases in cells. Next, a plasmid was used as a scaffold. In this case, the fluorophore and the quencher were attached to the same strand, and we expected that the dual-incision product containing them would be degraded in cells. At 3 h after transfection of HeLa cells with the plasmid-type probes, fluorescence emission was detected at the nuclei by fluorescence microscopy only when the probe contained the (6–4) photoproduct, and the results were confirmed by flow cytometry. Finally, XPA fibroblasts and the same cells expressing the *XPA* gene were transfected with the photoproduct-containing probe. Although the transfer of the probe into the cells was slow, fluorescence was detected depending on the NER ability of the cells.

Ultraviolet (UV) light causes photochemical reactions of the base moieties in DNA[1]. The major products are cyclobutane pyrimidine dimers (CPDs) and pyrimidine(6–4)pyrimidone photoproducts ((6–4) photoproducts), formed between adjacent pyrimidine bases. Since these photoproducts induce genetic mutations, which lead to carcinogenesis and cell death, they must be repaired by the nucleotide excision repair (NER) pathway to maintain genetic integrity[2]. The (6–4) photoproduct is repaired by NER more efficiently than the CPD[3], and other lesions that significantly alter the chemical structure of DNA, such as carcinogen adducts, are also removed by NER[4].

There are two subpathways in eukaryotic NER: global genome NER (GG-NER) and transcription-coupled NER (TC-NER)[2]. In GG-NER, the XPE protein, which consists of the DDB1 and DDB2 subunits, recognizes the lesion by forming a specific complex with damaged DNA[5], and then the DNA is transferred to the XPC protein, through the ubiquitylation of both proteins by the ubiquitin ligase bound to DDB1[6]. After this damage recognition step, TFIIH, a general transcription factor, and the XPA protein are recruited. TFIIH contains the XPB and XPD proteins, which both have DNA helicase activity, and the XPA protein is considered to stabilize the open complex and to verify the damage[2]. Subsequently, the ERCC1–XPF complex and the XPG protein, which are both structure-dependent nucleases, cleave the lesion-containing strand on the 5′ and 3′ sides of the damage site, respectively, to produce a fragment with a chain length of about 30 nucleotides. TC-NER differs from GG-NER only at the damage recognition step. This subpathway is initiated by the stalling of RNA polymerase II at the damage site, and other factors such as CSA and CSB are required, instead of the XPE and XPC proteins, to form the open complex containing the TFIIH complex and the XPA protein[7]. After the dual incisions by ERCC1–XPF and XPG, the repair is completed by DNA polymerase and DNA ligase.

Mutations in genes related to NER result in the diseases known as xeroderma pigmentosum (XP), Cockayne syndrome (CS), and trichothiodystrophy, which are autosomal recessive disorders[8,9]. Seven genes, *XPA–XPG*, which encode the proteins functioning in the NER pathway described above, were identified by complementation experiments, and the products of the CS-related genes are required to link the damage recognition to the open complex formation in the TCR subpathway. XP patients are extremely sensitive to sunlight and develop skin cancer at high rates[10,11]. The relative risks of non-melanoma skin cancer and melanoma in XP patients were

recently calculated to be about 10,000-fold and more than 2,000-fold higher, respectively, than those of the general population[12]. Neurological degeneration is also correlated with mutations in several XP genes[13].

Since XP is a hereditary disease in which skin cancer develops at an early age[12], its diagnosis is important. Based on the diagnosis, the patients are advised to avoid sunlight to prevent the onset of skin cancer. The most commonly used test is the measurement of unscheduled DNA synthesis (UDS)[10]. Skin fibroblast cultures are prepared from a biopsy obtained from the subject, and after irradiation with UV light, [^{3}H]thymidine incorporation into DNA is measured by autoradiography or liquid scintillation counting[14,15]. The XP cells show lower UDS ability, because the cells are deficient in the active proteins that recognize and remove the lesion. However, this diagnostic method is not entirely satisfactory, for several reasons. One is the risk of exposure of the medical staff to radiation in the use of the radioactive compound, although this problem may be solved by using a fluorescent nucleotide[16]. Another is the considerable suffering of the subject. In this study, we developed a fluorescent method for detecting the cellular ability to incise the damaged strand in the NER pathway, which could be applied to the screening of XP.

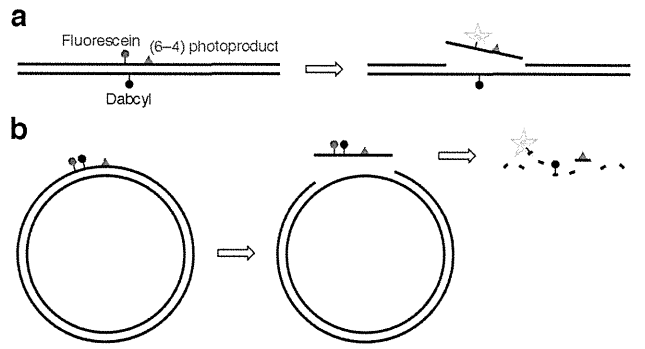

Figure 1 | Fluorescent probes to detect the NER dual incisions. (a) A linear duplex containing the (6–4) photoproduct and the fluorophore–quencher pair. Detection of the dual incisions in cells was not successful due to nonspecific degradation. (b) A plasmid-type probe containing the fluorophore and the quencher in the same strand. Degradation of the dual-incision product by cellular nucleases was expected to obtain the positive signal.

Results

Trial of linear DNA as a fluorescent probe. In our previous study[17], we developed fluorescent probes to detect base excision repair (BER), which initiates the removal of damaged bases with relatively small changes in their chemical structures. The probes were hairpin-shaped 30-mer oligonucleotides containing an oxidatively damaged base in the center, and bearing a fluorophore and a quencher at the 5′ and 3′ ends, respectively, in the same manner as a molecular beacon[18]. To detect the BER enzyme reaction in cells, nonspecific degradation was prevented by changing the phosphodiester linkages to nuclease-resistant phosphorothioate analogs in the regions that were not required for enzyme binding. We tried to use this system to detect the NER-specific dual incisions. However, the shortest substrate for NER reported so far was about 100 base-pair (bp) long[19], and a 140 bp duplex was used successfully to analyze NER *in vitro*[20], while the above-mentioned BER probe was composed of only 13 base pairs with a loop. Therefore, a strategy of attaching the fluorophore and the quencher to the base moieties in the central part of a long duplex was formulated, with the expectation that the fluorophore-tethered fragment would be released from the duplex after the dual incisions (Fig. 1a). Since the fluorophore and the quencher are generally attached to the end of the stem structure in molecular beacon-type probes, we firstly determined whether such internal labeling could function, using a short duplex shown in Supplementary Fig. S1a. When the two strands were mixed, the fluorescence intensity decreased, depending on the amount of the quencher-containing strand (Supplementary Fig. S1b).

Based on the above results, we designed a 140 bp duplex containing fluorescein, Dabcyl, and the (6–4) photoproduct, as shown in Supplementary Fig. S1c. Since little information is available about the protein–DNA interactions at the atomic level throughout the NER process, only three phosphodiester linkages at both ends in each strand were changed into phosphorothioates to protect the duplex from exonuclease digestion. A duplex containing normal thymines in place of the (6–4) photoproduct was also prepared, as a control. The duplexes with and without the (6–4) photoproduct were treated with a HEK293 cell extract, and the products were analyzed by PAGE. Replication protein A (RPA) was added to one of the reaction mixtures containing each duplex, because this factor reportedly facilitates NER[21]. A ladder of bands was obtained for the photoproduct-containing duplex, which was presumed to be produced by the dual incisions in the NER pathway. However, other bands were detected at the positions of 15- and 16-mers, in both the presence and absence of the (6–4) photoproduct (Supplementary Fig. S1d). Changes in the fluorescence intensity after a treatment with a HeLa cell extract were also analyzed. As expected from the PAGE results, no difference was observed between the duplexes with and without the photoproduct (Supplementary Fig. S1e). Finally, XPA cells, which are deficient in the NER activity, were transfected with these duplexes. Fluorescence was detected even when the duplex without the photoproduct was used (Supplementary Fig. S1f). These results suggested that the 140 bp duplexes were nonspecifically degraded during the incubation with the cell extracts or within the cells.

Plasmid-type fluorescent probe. Since the linear DNA was found to be too labile to be used as a fluorescent probe for the detection of cellular NER, even with the phosphorothioate modification at both ends, we tried a plasmid, which has often been used as a substrate for NER[21,22]. In the design of the plasmid-type probe, the fluorophore–quencher system was reconsidered. Since the linear probes were degraded nonspecifically in the cell extracts and in cells, we expected that the dual-incision product, which would be released from the plasmid as an oligonucleotide, would be degraded and fluoresce if the fluorophore and the quencher were attached at adjacent positions in this fragment (Fig. 1b). In preliminary experiments, oligonucleotides bearing fluorescein and Dabcyl at adjacent positions with no or one nucleotide insertion (Supplementary Fig. S2a) were prepared, and their properties were analyzed. When the Fl-Dab and Fl-T-Dab 28-mers in Supplementary Fig. S2a were hybridized to the complementary 28-mer, the quenching efficiencies were 99 and 98%, respectively. Quenching occurred very efficiently even in the single-stranded form (at 0 min in Supplementary Fig. S2b), and the fluorescence intensity increased upon treatment with a HeLa cell extract. Fluorescence was also observed in the cells transfected with these oligonucleotides (Supplementary Fig. S2c). Since the fluorescence intensity was increased more efficiently when an extra nucleotide was inserted between the fluorophore and the quencher (Supplementary Fig. S2b), we adopted this system, and prepared a plasmid designated as pBSII KS (-) FQ64 (Fig. 2a). A 9 bp sequence was inserted into the original plasmid, pBSII KS (-) UV[23], to incorporate the modified thymidines bearing the fluorophore and the quencher, and the single-stranded DNA was prepared using VCS-M13 helper phage. A 37-mer oligonucleotide containing the (6–4) photoproduct and the modified thymidines (Fig. 2b) was hybridized to this DNA, and pBSII KS (-) FQ64 was obtained using DNA polymerase and DNA ligase. pBSII KS (-) FQTT, which contained undamaged thymine bases in place of the (6–4) photoproduct, was also prepared as a negative-control probe. The presence of the (6–4) photoproduct in pBSII KS (-) FQ64 was

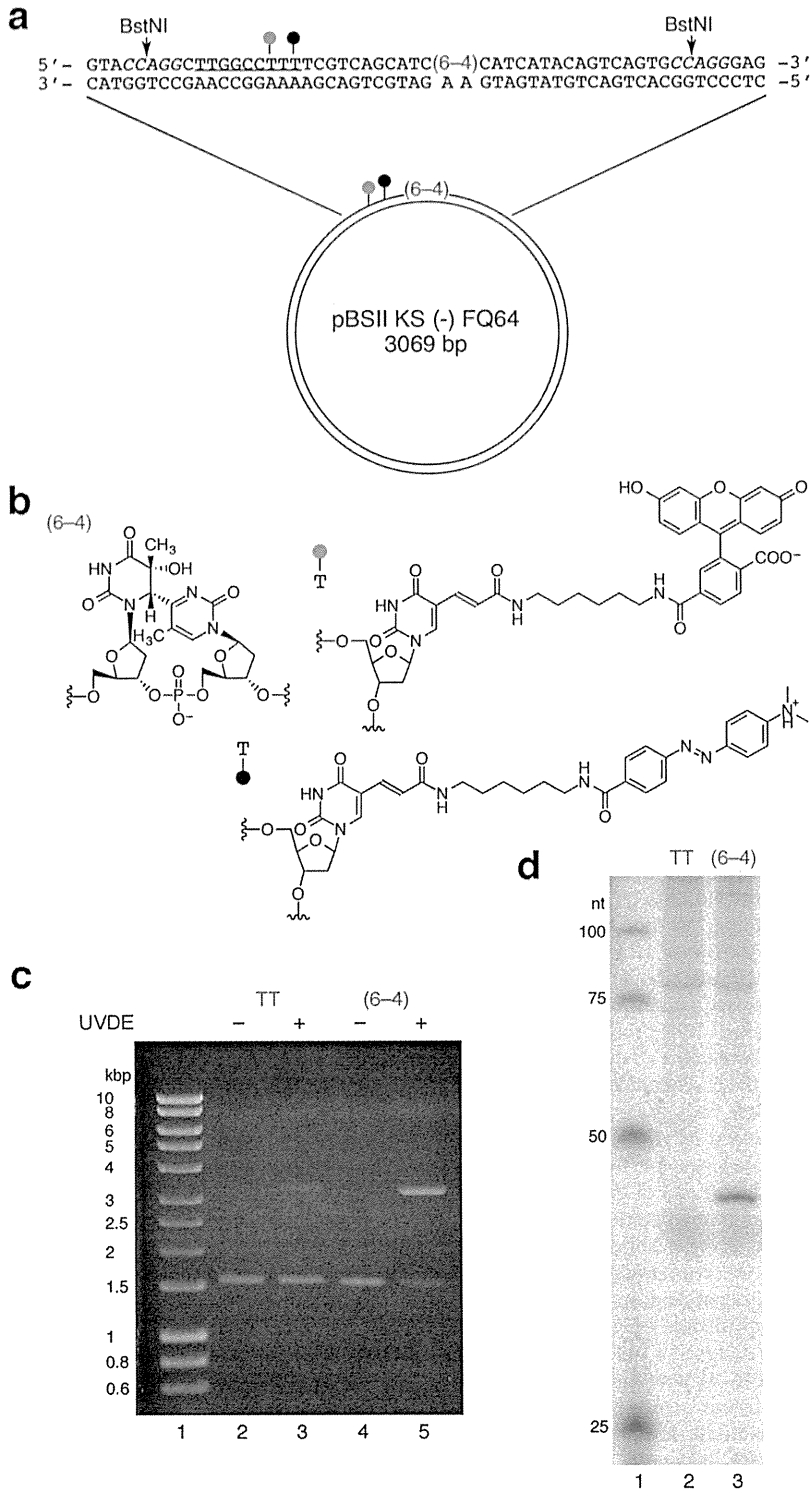

Figure 2 | Plasmid-type fluorescent probe to detect the NER dual incisions. (a) Structure of the plasmid. The green and black circles represent fluorescein and Dabcyl, respectively. The italicized letters represent the BstNI recognition sequence, and the underlined sequence was added to the original pBSII KS (-) UV plasmid[23] to incorporate the modified nucleosides. (b) Chemical structures of the (6–4) photoproduct and the modified nucleosides bearing fluorescein and Dabcyl. (c) UVDE treatment of pBSII KS (-) FQTT (TT) and pBSII KS (-) FQ64 ((6–4)). (d) Repair synthesis on pBSII KS (-) FQTT (TT) and pBSII KS (-) FQ64 ((6–4)), followed by BstNI digestion.

confirmed by UVDE digestion (Fig. 2c) and the repair synthesis in NER (Fig. 2d).

Fluorescence detection of NER in cells. HeLa cells were transfected with either pBSII KS (-) FQ64 or pBSII KS (-) FQTT, using Lipofectamine 2000. A transfection reporter bearing Cy5, which was developed in our previous study[24], was co-transfected to prevent false negative results, although its structure was substantially different from that of the probe. At 3 h after transfection, the fluorescein emission was detected at the nuclei, depending on the presence of the photoproduct (Fig. 3a). The Cy5 emission in the cells transfected with pBSII KS (-) FQTT demonstrated that the result obtained for these cells was not falsely negative.

To obtain more quantitative information, the cellular NER reaction was analyzed by flow cytometry. HeLa cells were transfected with pBSII KS (-) FQ64 or pBSII KS (-) FQTT, together with the transfection reporter, in the same manner as above. At 1 h intervals, the cells were harvested by trypsin digestion, and analyzed on a flow cytometer. The Cy5 emission from the transfection reporter was the same between the pBSII KS (-) FQ64- and pBSII KS (-) FQTT-transfected cells, and the transfer of the probes into the cells was apparently completed at 3 h after the transfection (Fig. 3b, lower panels). At this time, a difference in the fluorescein emission was observed between the cells transfected with the probes with and without the (6–4) photoproduct, and this difference disappeared at 4 h, probably due to the nonspecific degradation of the probes (Fig. 3b, upper panels). These results demonstrated that cellular NER could be monitored by flow cytometry, although the background was relatively high at the fluorescein emission wavelength (Supplementary Fig. S3).

Finally, the XPA fibroblasts that were deficient in the NER activity (XP12ROSV) and the same cells in which the *XPA* gene was expressed (XP12ROSV/XPA)[25] were transfected with pBSII KS (-) FQ64. In this case, a longer culture time was required because the transfer of the probe into the cells was apparently slower, as determined by the Cy5 emission from the transfection reporter. However, positive signals were observed only in the experiments using the NER-proficient cells (Fig. 4a). The fluorescence intensities in the microscopic images of the cells were quantified (Fig. 4b), and a significant difference was found between the NER-deficient and -proficient cells, although the background fluorescence, which was observed in the flow cytometry analysis (Supplementary Fig. S3), was included.

Discussion

In this study, we intended to develop a fluorescent probe to detect cellular NER, for possible use in the diagnosis of XP. At first, we tried to apply our study on the BER probe, a short hairpin oligonucleotide that emits fluorescence upon strand scission by DNA glycosylase/AP lyase[17]. However, there was a problem that the substrate for NER must be much longer than that for BER[19,20]. Since the molecular beacon-type fluorophore–quencher system[18] could be used when

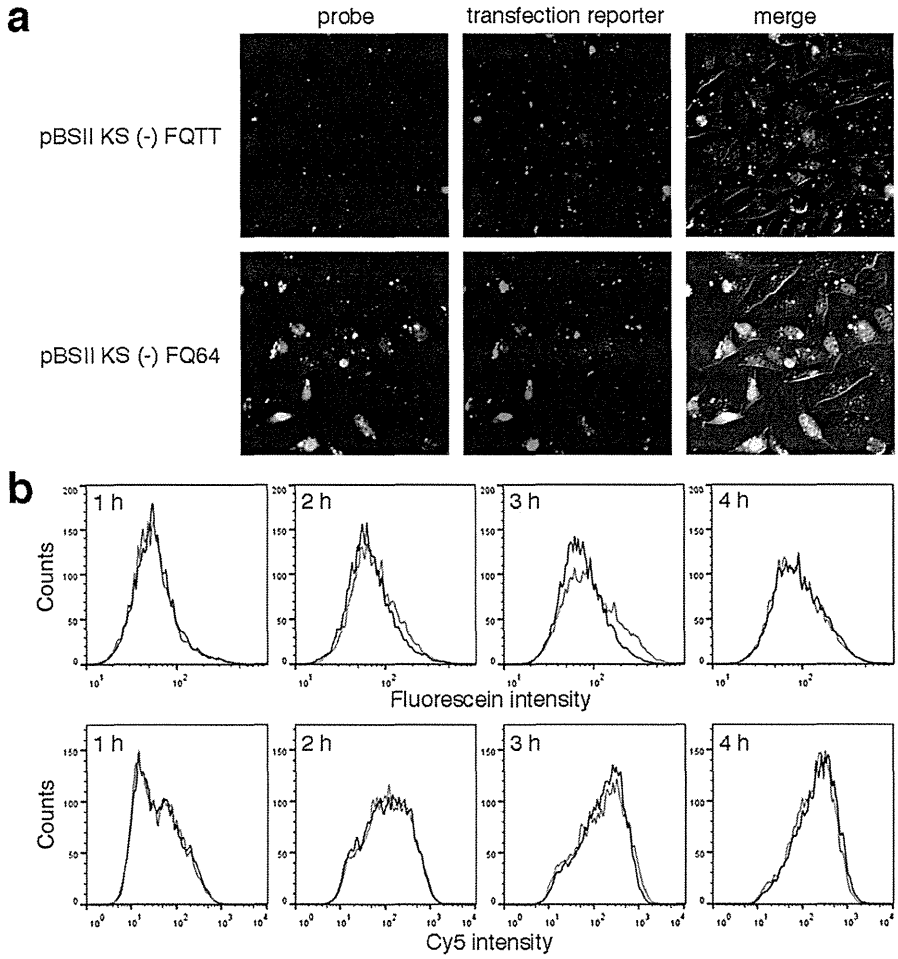

Figure 3 | Detection of the NER dual incisions in HeLa cells. (a) Fluorescence images of the cells cultured at 37°C for 3 h, after transfection with pBSII KS (-) FQTT (upper panels) or pBSII KS (-) FQ64 (lower panels). (b) Flow cytometry analysis of the HeLa cells transfected with pBSII KS (-) FQTT (blue) or pBSII KS (-) FQ64 (red), together with the transfection reporter bearing Cy5[24].

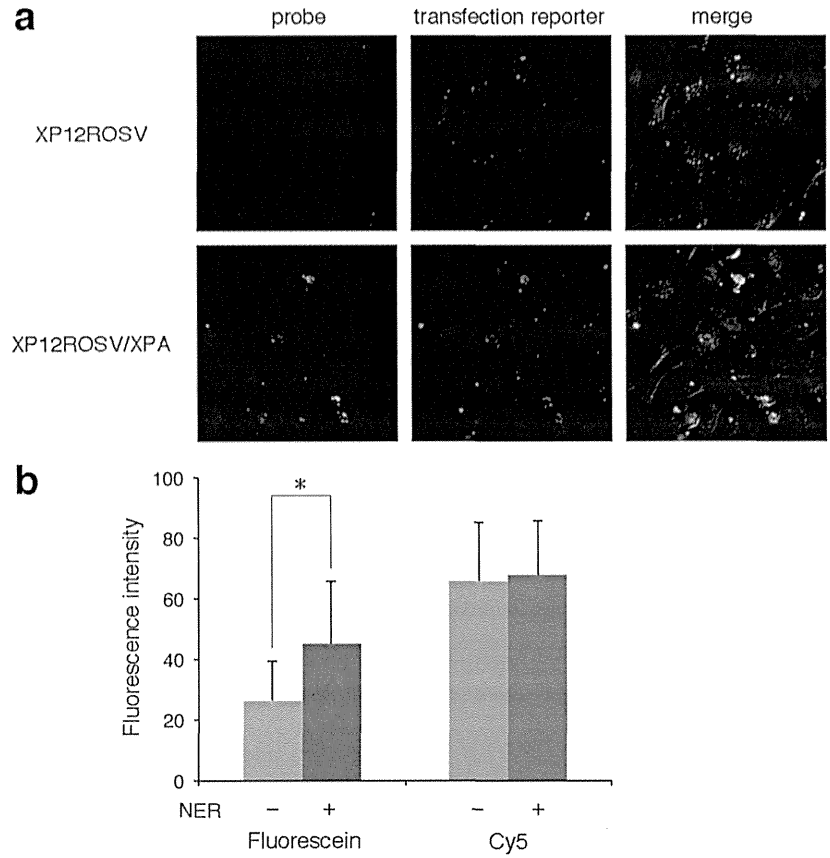

Figure 4 | Detection of the cellular NER ability. (a) The XPA cells (upper panels) and the same cells in which the *XPA* gene was expressed (lower panels) were cultured at 37°C for 6 h after transfection with pBSII KS (-) FQ64. (b) The fluorescein and Cy5 emissions from the pBSII KS (-) FQ64 probe and the transfection reporter, respectively, in the XP12ROSV (NER −) and XP12ROSV/XPA (NER +) cells, shown in panel a, were quantified. The data were statistically analyzed by Student's t test ($n = 10$; *, $p < 0.01$), and error bars represent standard deviation. Background correction was not performed.

the two dyes were tethered to the base moieties in the inner region of each strand (Supplementary Figs. S1a and S1b), a 140 bp duplex containing the (6–4) photoproduct (Supplementary Fig. S1c), which is known as a good substrate for NER[3], was tested. Contrary to our expectations, degradation of the duplex was observed in *in vitro* and *ex vivo* experiments (Supplementary Figs. S1d–f). Therefore, we used a plasmid as a scaffold, and reexamined the fluorophore–quencher system to utilize the nuclease degradation of the probe. The structure of the plasmid in which the fluorophore and the quencher were attached to the same strand (Fig. 2a) facilitated the preparation of the probe, because only the DNA polymerase and DNA ligase reactions were required after a modified oligonucleotide primer was synthesized.

At 3 h and 6 h after transfection of the HeLa cells and the XPA fibroblasts, respectively, fluorescein fluorescence was detected, depending on the presence of the (6–4) photoproduct and the cellular NER ability (Figs. 3a and 4a). Therefore, these signals were attributed to the degradation of the dual-incision fragment produced by NER. At a longer culture time, nonspecific degradation of the plasmid was observed, as detected by flow cytometry (4 h in Fig. 3b). Therefore, control experiments using the plasmid without the (6–4) photoproduct were important. The transfection reporter developed in our previous study[24] was also useful to distinguish between the true- and false-negative results. Interestingly, we always observed fluorescence emission from the nuclei. Several types of fluorescent probes were developed to visualize the nuclease degradation of DNA in cells[26,27], and our plasmid that lacks the (6–4) photoproduct can be used for this purpose. The half-life of plasmid DNA microinjected into the cytosol is reportedly 50–90 min[28], but we never observed fluorescence in the cytosol, suggesting that our probe, which was transferred into the cells using a cationic lipid, was transported into the nuclei, although no nuclear targeting strategy[29] was used.

Recently, Sancar and co-workers investigated the fate of the fragments produced by the dual incisions in NER[30,31]. Their *in vitro* study[30] revealed that the photoproduct is removed in the form of a 30-mer oligonucleotide in complex with TFIIH. The oligonucleotide is dissociated from TFIIH in an ATP-dependent manner, and then RPA binds to the DNA fragment. It was suggested that the RPA protects this oligomer from degradation by nuclease digestion. From our results, however, the dual-incision product appeared to be quite labile in cells. Degradation products shorter than 20-nucleotide long were detected after incubation for 1 h or longer in their study[30], and the fluorophore was not located close to the (6–4) photoproduct in our probe. Therefore, the protection by RPA seems to have limited effects at least at the ends of the dual-incision fragment.

Our fluorescent probe may be applied to the screening of XP, which is a hereditary disease caused by cellular NER deficiency. For use as an alternative to the UDS measurement for the diagnosis of XP, the transfection efficiency into fibroblasts or the quantum yield of fluorescence should be improved by changing the transfection reagent or the fluorophore, because the fluorescence intensity was low when the XPA fibroblasts were used (Fig. 4a). Our probe can also be used to compare two types of lesions as substrates for NER in a single cell. When cells are transfected with two plasmids, each containing an individual set of the lesion and the fluorophore, the

better substrate can be determined by observing the fluorescence at two wavelengths. Artificial substrates for NER were reported recently[32]. If this method reveals that they are better substrates than the (6–4) photoproduct, then their incorporation into the plasmid may improve the sensitivity of the probe. Another benefit of our method, in which cells are not irradiated with UV, is that only the cellular GG-NER process is monitored, and thus other effects of UV-related reactions, such as lipid oxidation, are avoided. Therefore, our probe will contribute to both medical and biological studies.

Methods

Synthesis of oligonucleotides. The phosphoramidite building block of the (6–4) photoproduct was synthesized by the previously described method[33]. To incorporate the fluorescein- and Dabcyl-tethered nucleosides, Fluorescein-dT Phosphoramidite and Dabcyl-dT were purchased from Glen Research. Oligonucleotides were synthesized on an Applied Biosystems 3400 DNA synthesizer. Benzimidazolium triflate was used as an activator for the synthesis of the (6–4) photoproduct-containing oligonucleotide[34]. After deprotection, the products were purified by HPLC, using a Waters μ-Bondasphere C18 5 μm 300 A column (3.9 × 150 mm) with a linear gradient of acetonitrile in 0.1 M triethylammonium acetate (pH 7.0) at a flow rate of 1.0 ml/min. The transfection reporter was synthesized as described previously[24].

Preparation of 140 bp duplexes. For the analysis of the dual incisions by gel electrophoresis, 14-mers (20 pmol) with and without the (6–4) photoproduct, d(CGCGAATTGCGCCC), in which the photoproduct site is underlined, were incubated with [γ-^{32}P]ATP (3.7 MBq) and T4 polynucleotide kinase (Takara Bio) (10 units), in buffer (50 μl) containing 50 mM Tris-HCl (pH 8.0), 10 mM $MgCl_2$, and 5 mM DTT, at 37°C for 30 min. After heating at 95°C for 5 min, the products were purified using an illustra MicroSpin G-25 column (GE Healthcare). Aliquots of each 5′-phosphorylated 14-mer (4.8 pmol) were mixed with four oligonucleotides, d(GsAsCsCTGAACACGTACGGAATTCGATATCCTCGAGCCAGATCT-GCGCCAGTTGGCCXACTCGTC) (7.2 pmol), in which s and X represent the phosphorothioate linkage and the fluorescein-tethered nucleoside (Fig. 2b), respectively, p-d(ACAGTCAGTGGCTTGGGCTGCAGCAGGTCGACTCTA-GAGGATCCCGGGCGAGCTCGAATTsCsGsC) (7.2 pmol), in which p represents the terminal phosphate, d(TTCGCGGACGAGTAGG) (10 pmol), and d(CACTGACTGTGGGCGC) (10 pmol), in buffer (58 μl) containing 10 mM Tris-HCl (pH 7.9), 50 mM NaCl, 10 mM $MgCl_2$, and 1 mM DTT. The mixtures were heated at 95°C for 2 min, and gradually cooled to 25°C during 45 min. After ATP (12 nmol) and T4 DNA ligase (Takara Bio) (210 units) were added, the mixtures were incubated at 16°C overnight, and then heated at 75°C for 10 min. The products were purified by 10% denaturing PAGE, and desalted using the MicroSpin G-25 column. For fluorescence detection, 10 nmol of the 14-mer was phosphorylated in buffer (100 μl) using ATP (0.2 μmol) and T4 polynucleotide kinase (100 units), and the ligation was performed in buffer (100 μl), using 12 nmol of the 5′- and 3′-side oligonucleotides, 20 nmol of the splint 16-mers, and 3,500 units of T4 DNA ligase, in the presence of 1 mM ATP. The complementary strand was prepared using d(GsCsGsAATTCGAGCTCGCCCGGGATCCTCTAGAGTCGACCTGCTGC-AGCCCAAGCCACTGACTGTGGGCGCAAT) (10 nmol), p-d(TCGCGGA-CGAGYAGGCCAACTGGCGCAGATCTGGCTCGAGGATATCGAATTCCG-TACGTGTTCAGsGsTsC) (10 nmol), in which Y represents the Dabcyl-tethered nucleoside (Fig. 2b), and d(GTCCGCGAATTGCGCC) (20 nmol), in the same manner. The amounts of the 140-mer oligonucleotides obtained after the PAGE purification were determined by the radioactivity and the UV absorption, in the cases of the ^{32}P labeling and the large-scale preparation, respectively. The 140 bp duplex (Supplementary Fig. S1c) was formed by mixing the fluorescein-containing strand with a 1.25-fold amount of the Dabcyl-containing strand, in buffer containing 10 mM Tris-HCl (pH 8.0) and 50 mM NaCl, followed by heating at 95°C for 2 min and cooling to 25°C during 45 min.

Experiments using the 140 bp duplexes. Dual-incision assays (Supplementary Fig. S1d) were performed according to the described method[35], using the ^{32}P-labeled 140 bp duplexes with and without the (6–4) photoproduct (35 fmol) and the whole cell extracts[36] in 50 μl solutions for 2 h, followed by 14% denaturing PAGE and band detection with a Typhoon FLA 7000 image analyzer (GE Healthcare). Fluorescence intensities (Supplementary Fig. S1e) were measured at 37°C, using the same assay solutions after dilution to 200 μl with 1 M Tris-HCl (pH 8.0), on a JASCO FP-6500 spectrofluorometer equipped with an EHC 573 temperature controller. The excitation and emission wavelengths were 494 and 520 nm, respectively, with bandwidths of 3 nm. For the transfection of the XP12ROSV cells[25] (Supplementary Fig. S1f), the cells were grown in Dulbecco's modified Eagle's medium (DMEM) supplemented with 15% fetal bovine serum, 100 units/ml penicillin, and 100 μg/ml streptomycin at 37°C in a humidified 5% CO_2 incubator. The cells were seeded into a 4-well slide lumox (Greiner Bio-One), grown to about 90% confluence, and transfected with the 140 bp duplexes using Lipofectamine 2000 (Life Technologies), according to the manufacturer's instructions. At 6 h after transfection, the cells were analyzed with an Olympus IX71 fluorescence microscopy system.

Preparation of the plasmid-type probes. A 9-nucleotide sequence for the incorporation of the modified nucleosides was inserted into pBSII KS (-) UV[23], using two primers, d(CGAAAAGGCCAAGCCTGGTACCCAGCTTTT) and d(GGCTTGGCCTTTTCGTCAGCATCTTCATCA), in which the inserted sequences are underlined, a PrimeSTAR Mutagenesis Basal Kit (Takara Bio), and HIT-JM109 competent cells (RBC Bioscience), according to the manufacturers' instructions. A single colony, cultured at 37°C for 1 day in Lysogeny Broth medium (4 ml) containing ampicillin, was diluted with the same medium (400 ml), and VCS-M13 helper phage (Stratagene) was added at a concentration of $>1.0 \times 10^{11}$ pfu/ml. After an incubation at 37°C for 1 day, the single-stranded DNA was obtained, as described previously[37]. The probes, pBSII KS (-) FQ64 (Fig. 2a) and pBSII KS (-) FQTT, were prepared from this DNA using a primer, p-d(AGGCTTGGCC-XTYTCGTCAGCATCTTCATCATACAGT), in which X and Y represent the fluorescein- and Dabcyl-tethered nucleosides (Fig. 2b), with and without the (6–4) photoproduct at the underlined site, as described previously[35].

UVDE treatment. pBSII KS (-) FQ64 and pBSII KS (-) FQTT (250 ng) were incubated with *Schizosaccharomyces pombe* UVDE (Trevigen) (1 μl), in buffer (20 μl) containing 20 mM HEPES-KOH (pH 6.5), 10 mM $MgCl_2$, 1 mM $MnCl_2$, and 100 mM NaCl, at 30°C for 1 h. After the addition of loading buffer (2 μl) containing 25% Ficoll, 2% SDS, and 10 mM EDTA (pH 8.0), the products were analyzed by 1% agarose gel electrophoresis, followed by visualization of the bands with ethidium bromide.

Repair synthesis. pBSII KS (-) FQ64 and pBSII KS (-) FQTT (150 ng) were incubated with a HeLa whole cell extract[36] (86 μg) and [α-^{32}P]dCTP (15 kBq), in a solution (10 μl) containing 50 mM HEPES-KOH (pH 7.8), 70 mM KCl, 9.8 mM $MgCl_2$, 1.3 mM DTT, 2 mM ATP, 1 μM dNTP (N = A, G, T), 0.1 μM dCTP, 22 mM phosphocreatine, 0.2 mM glycine, 0.4 mM EDTA, 0.36 mg/ml BSA, 50 μg/ml creatine phosphokinase, and 7.8% glycerol, at 30°C for 1 h. To this solution, 0.5 M EDTA (2 μl), 10% SDS (3 μl), and proteinase K (Invitrogen) (20 μg) were added, and the mixtures were incubated at 56°C for 20 min. After phenol-chloroform extraction and ethanol precipitation, the DNA was incubated with BstNI (New England Biolabs) (5 units), in buffer (10 μl) containing 10 mM Tris-HCl (pH 7.9), 10 mM $MgCl_2$, 50 mM NaCl, 1 mM DTT, and 100 μg/ml BSA, at 60°C for 1 h. The products were analyzed by 12.5% denaturing PAGE, and the bands were detected with the FLA 7000 image analyzer.

Transfection of the cells and fluorescence detection. HeLa S3, XP12ROSV, and XP12ROSV/XPA cells were grown in DMEM supplemented with 15% fetal bovine serum, 100 units/ml penicillin, and 100 μg/ml streptomycin, at 37°C in a humidified 5% CO_2 incubator. The cells were seeded into 24-well plates (Trueline), grown to about 90% confluence, and transfected with pBSII KS (-) FQ64 or pBSII KS (-) FQTT (20 μg), which was mixed with the transfection reporter[24] (10 pmol), using Lipofectamine 2000 (Life Technologies), according to the manufacturer's instructions. At the described intervals after transfection, the cells were analyzed with the Olympus IX71 fluorescence microscopy system. The fluorescence intensities of 10 cells in Fig. 4a were quantified and averaged, using the ImageJ software (National Institutes of Health).

Flow cytometry. HeLa cells were cultured and transfected with the probes, in the same manner as described above. After 1, 2, 3, and 4 h, the culture medium was removed, and the cells were washed with phosphate-buffered saline (PBS). The cells were harvested by trypsin digestion, and suspended in DMEM (2 ml). The suspension was centrifuged at 1,000 rpm for 3 min, and the cell pellet was mixed with 4% paraformaldehyde phosphate buffer solution (1 ml). After 30 min at room temperature, the cells were collected by centrifugation at 1,000 rpm for 3 min, washed with PBS (1 ml), and suspended in PBS (1 ml). The samples were prepared by passing the cells through a cell strainer (BD Falcon). The analysis was performed on a BD Biosciences FACSCalibur flow cytometer controlled by the CellQuest software, version 3.3. The fluorescein and Cy5 emissions were detected using the FL1 and FL3 filters, respectively, and each measurement was performed using 10,000 cells. Each data set was analyzed using the FlowJo software. To reduce the background signal, the gating of the cells was set to analyze more than 96.7% of the total cells.

1. Iwai, S. Pyrimidine dimers: UV-induced DNA damage. In *Modified Nucleosides in Biochemistry, Biotechnology and Medicine: Wiley-VCH*, 97–131 (2008).
2. Naegeli, H. & Sugasawa, K. The xeroderma pigmentosum pathway: decision tree analysis of DNA quality. *DNA Repair* **10**, 673–683 (2011).
3. Szymkowski, D. E., Lawrence, C. W. & Wood, R. D. Repair by human cell extracts of single (6-4) and cyclobutane thymine-thymine photoproducts in DNA. *Proc. Natl. Acad. Sci. U.S.A.* **90**, 9823–9827 (1993).
4. Li, C., Wang, L.-E. & Wei, Q. DNA repair phenotype and cancer susceptibility – a mini review. *Int. J. Cancer* **124**, 999–1007 (2009).
5. Scrima, A. *et al.* Structural basis of UV DNA-damage recognition by the DDB1–DDB2 complex. *Cell* **135**, 1213–1223 (2008).
6. Sugasawa, K. *et al.* UV-induced ubiquitylation of XPC protein mediated by UV-DDB-ubiquitin ligase complex. *Cell* **121**, 387–400 (2005).
7. Fousteri, M. & Mullenders, L. H. F. Transcription-coupled nucleotide excision repair in mammalian cells: molecular mechanisms and biological effects. *Cell Res.* **18**, 73–84 (2008).

8. Cleaver, J. E., Lam, E. T. & Revet, I. Disorders of nucleotide excision repair: the genetic and molecular basis of heterogeneity. *Nat. Rev. Genet.* **10**, 756–768 (2009).
9. Thoms, K.-M., Kuschal, C. & Emmert, S. Lessons learned from DNA repair defective syndromes. *Exp. Dermatol.* **16**, 532–544 (2007).
10. Lehmann, A. R., McGibbon, D. & Stefanini, M. Xeroderma pigmentosum. *Orphanet J. Rare Dis.* **6**, 70 (2011).
11. DiGiovanna, J. J. & Kraemer, K. H. Shining a light on xeroderma pigmentosum. *J. Invest. Dermatol.* **132**, 785–796 (2012).
12. Bradford, P. T. *et al.* Cancer and neurologic degeneration in xeroderma pigmentosum: long term follow-up characterises the role of DNA repair. *J. Med. Genet.* **48**, 168–176 (2011).
13. Nouspikel, T. Nucleotide excision repair and neurological diseases. *DNA Repair* **7**, 1155–1167 (2008).
14. Stefanini, M. *et al.* Differences in the levels of UV repair and in clinical symptoms in two sibs affected by xeroderma pigmentosum. *Human Genet.* **54**, 177–182 (1980).
15. Lehmann, A. R. & Stevens, S. A rapid procedure for measurement of DNA repair in human fibroblasts and for complementation analysis of xeroderma pigmentosum cells. *Mutat. Res.* **69**, 177–190 (1980).
16. Limsirichaikul, S. *et al.* A rapid non-radioactive technique for measurement of repair synthesis in primary human fibroblasts by incorporation of ethynyl deoxyuridine (EdU). *Nucleic Acids Res.* **37**, e31 (2009).
17. Matsumoto, N. *et al.* Fluorescent probes for the analysis of DNA strand scission in base excision repair. *Nucleic Acids Res.* **38**, e101 (2010).
18. Tyagi, S. & Kramer, F. R. Molecular beacons: probes that fluoresce upon hybridization. *Nat. Biotechnol.* **14**, 303–308 (1996).
19. Huang, J.-C. & Sancar, A. Determination of minimum substrate size for human excinuclease. *J. Biol. Chem.* **269**, 19034–19040 (1994).
20. Matsunaga, T., Mu, D., Park, C.-H., Reardon, J. T. & Sancar, A. Human DNA repair excision nuclease: analysis of the roles of the subunits involved in dual incisions by using anti-XPG and anti-ERCC1 antibodies. *J. Biol. Chem.* **270**, 20862–20869 (1995).
21. Rapić Otrin, V. *et al.* Relationship of the xeroderma pigmentosum group E DNA repair defect to the chromatin and DNA binding proteins UV-DDB and replication protein A. *Mol. Cell. Biol.* **18**, 3182–3190 (1998).
22. Moggs, J. G., Yarema, K. J., Essigmann, J. M. & Wood, R. D. Analysis of incision sites produced by human cell extracts and purified proteins during nucleotide excision repair of a 1,3-intrastrand d(GpTpG)-cisplatin adduct. *J. Biol. Chem.* **271**, 7177–7186 (1996).
23. Mei Kwei, J. S. *et al.* Blockage of RNA polymerase II at a cyclobutane pyrimidine dimer and 6–4 photoproduct. *Biochem. Biophys. Res. Commun.* **320**, 1133–1138 (2004).
24. Toga, T., Kuraoka, I., Yasui, A. & Iwai, S. A transfection reporter for the prevention of false-negative results in molecular beacon experiments. *Anal. Biochem.* **440**, 9–11 (2013).
25. Hasegawa, M., Iwai, S. & Kuraoka, I. A non-isotopic assay uses bromouridine and RNA synthesis to detect DNA damage responses. *Mutat. Res.* **699**, 62–66 (2010).
26. Srinivasan, C., Siddiqui, S., Silbart, L. K., Papadimitrakopoulos, F. & Burgess, D. J. Dual fluorescent labeling method to visualize plasmid DNA degradation. *Bioconjug. Chem.* **20**, 163–169 (2009).
27. Gong, P. *et al.* DNase-activatable fluorescence probes visualizing the degradation of exogenous DNA in living cells. *Nanoscale* **4**, 2454–2462 (2012).
28. Lechardeur, D. *et al.* Metabolic instability of plasmid DNA in the cytosol: a potential barrier to gene transfer. *Gene Ther.* **6**, 482–497 (1999).
29. Wagstaff, K. M. & Jans, D. A. Nucleocytoplasmic transport of DNA: enhancing non-viral gene transfer. *Biochem. J.* **406**, 185–202 (2007).
30. Kemp, M. G., Reardon, J. T., Lindsey-Boltz, L. A. & Sancar, A. Mechanism of release and fate of excised oligonucleotides during nucleotide excision repair. *J. Biol. Chem.* **287**, 22889–22899 (2012).
31. Hu, J. *et al.* Nucleotide excision repair in human cells: fate of the excised oligonucleotide carrying DNA damage in vivo. *J. Biol. Chem.* **288**, 20918–20926 (2013).
32. Evdokimov, A. *et al.* New synthetic substrates of mammalian nucleotide excision repair system. *Nucleic Acids Res.* **41**, e123 (2013).
33. Iwai, S., Shimizu, M., Kamiya, H. & Ohtsuka, E. Synthesis of a phosphoramidite coupling unit of the pyrimidine (6-4) pyrimidone photoproduct and its incorporation into oligodeoxynucleotides. *J. Am. Chem. Soc.* **118**, 7642–7643 (1996).
34. Iwai, S. *et al.* Benzimidazolium triflate-activated synthesis of (6–4) photoproduct-containing oligonucleotides and its application. *Nucleic Acids Res.* **27**, 2299–2303 (1999).
35. Shivji, M. K. K., Moggs, J. G., Kuraoka, I. & Wood, R. D. Dual-incision assays for nucleotide excision repair using DNA with a lesion at a specific site. *Methods Mol. Biol.* **113**, 373–392 (1999).
36. Manley, J. L., Fire, A., Cano, A., Sharp, P. A. & Gefter, M. L. DNA-dependent transcription of adenovirus genes in a soluble whole-cell extract. *Proc. Natl. Acad. Sci. U.S.A.* **77**, 3855–3859 (1980).
37. Green, M. R. & Sambrook, J. Preparation of single-stranded bacteriophage M13 DNA by precipitation with polyethylene glycol. In *Molecular Cloning: A Laboratory Manual, 4th Ed.: Cold Spring Harbor Laboratory Press*, 31–33 (2012).

Acknowledgments

This study was supported by a Grant-in-Aid for Scientific Research from the Ministry of Education, Culture, Sports, Science, and Technology of Japan (233948 to T.T.). T.T. was supported by a Research Fellowship for Young Scientists from the Japan Society for the Promotion of Science.

Author contributions

S.I. and C.N. designed research; T.T., I.K., S.W., E.N., S.T. and K.S. performed research; I.K. and S.T. analyzed data; S.I. wrote the paper.

Additional information

Supplementary information accompanies this paper at http://www.nature.com/scientificreports

Competing financial interests: The authors declare no competing financial interests.

How to cite this article: Toga, T. *et al.* Fluorescence detection of cellular nucleotide excision repair of damaged DNA. *Sci. Rep.* 4, 5578; DOI:10.1038/srep05578 (2014).

CHAPTER 19

PHOTOCARCINOGENESIS AND INFLAMMATION

Chikako Nishigori

There is ample evidence demonstrating that solar ultraviolet (UV) light induces human skin cancers. First, epidemiological studies have demonstrated a negative correlation between the latitude of residence and incidence and mortality rates of skin cancer in homogeneous populations (1,2). Second, skin cancer can be produced in mice by UV irradiation; the action spectrum of photocarcinogenesis falls into UVB (280 to 320 nm) (3,4). Third, patients with genetic disorders that lead to deficiencies in repairing UV-induced DNA damage are prone to develop cancers in sun-exposed areas of the skin (5).

Accumulation of DNA lesions in several genes, such as oncogenes and tumor suppressor genes, plays a crucial role in carcinogenesis. UV irradiation causes DNA lesions, which are thought to be responsible for sunlight-induced skin cancers. Indeed, even in actinic keratosis, precancerous lesions of squamous cell caricinoma (SCC), genetic alterations can be observed (6).

UVB-induced skin cancer development (photocarcinogenesis) is a complex multistage process that involves initiation, promotion, and progression. Each of these processes is mediated by various cellular, biochemical, and molecular changes. The pyrimidine photoproducts that result from direct DNA damage induced by UV are an important cause of skin cancer. DNA damage induces mutations that lead to the up- or down-regulation of signal transduction pathways, cell-cycle dysregulation, and depletion of antioxidant defenses (6,7). In addition to these changes, UVB-induced immunosuppression also plays an important role in photocarcinogenesis (8,9).

Chronic inflammation is induced by various environmental factors, including sunlight. Epidemiological and experimental studies have indicated that chronic inflammation is closely involved in human carcinogenesis. Epidemiological studies have shown that acute intense exposure to UV rays is also a major risk factor for developing skin cancer, implying that intermittent severe inflammation caused by acute sunburn is an important factor in the development of skin cancers.

Cancer and Inflammation Mechanisms: Chemical, Biological, and Clinical Aspects, First Edition.
Edited by Yusuke Hiraku, Shosuke Kawanishi, and Hiroshi Ohshima.

DNA DAMAGE CAUSED BY SUNLIGHT

UV wavelengths from the Sun that reach the surface of the Earth are UVA (320 to 400 mm) and part of UVB (280 to 320 nm) because UV wavelengths below 300 nm are absorbed by the ozone layer. Irradiation with UVA or UVB results in the production of reactive oxygen species (ROSs). However, because the absorbance spectrum of DNA extends well into the UVB range, DNA absorbs more UVB photon energy directly than UVA. Therefore, UVB acts on DNA by exciting the nucleobases directly, resulting in the formation of dimeric photoproducts at dipyrimidine sites in an oxygen-independent manner. Comparatively, UVA and visible light tend to participate in the formation of ROSs in the presence of photosensitizers (10,11) irrespective of the involvement of oxygen. UVB not only produces pyrimidine dimers and (6-4) photoproducts (6-4 PPs) by direct excitation, but also produces ROSs in the presence of photosensitizers, which cause oxidative DNA damage. Previous studies have suggested that dipyrimidine photoproducts are the major molecule among UV-induced DNA lesions involved in cytotoxicity and mutagenesis (12).

On the other hand, ROSs cause various biological effects via the redox-signaling pathway (13) and oxidative DNA damage and thus play a role in carcinogenesis (14). Several types of modified DNA are produced by ROSs. Among them, 8-hydroxydeoxyguanosine (8-OHdG) has been established as a sensitive marker of oxidative DNA damage. It can be generated in the presence of a photosensitizer either electron transfer or by hydroxy radicals and singlet oxygen ($^1O_2$) with oxygen molecules. 8-OHdG is generated in fibroblasts derived from human skin in response to exposure to artificial light sources such as sunlamps (UVB) or monochromatic radiation ranging from 312 nm up to near visible (434 nm). Kvam and Tyrrell analyzed the spectrum for the yield of oxidative damage in confluent, nongrowing, primary skin fibroblasts, and they determined that UVA and near-visible radiation cause almost all of the guanine oxidation (10). Ito et al. reported that the photodynamic action of riboflavin caused the formation of 8-OHdG in double-stranded DNA and that no enhancing effect by D_2O was observed (15), suggesting that $^1O_2$ molecules were not involved. The estimated ratio of 8-OHdG yield to total guanine loss indicated that the photoexcited riboflavin specifically induced 8-OHdG formation at the guanine residues located 5′ to another guanine by electron transfer. The guanine base in genomic DNA is highly susceptible to oxidative stress, as it possesses the lowest oxidation potential of all the bases. Besaratinia reported that UVA irradiation at a dose of 18 J/cm^2 produced significant levels of 8-oxo-2′-deoxyguanosine (8-oxodG) in DNA, and UVA-induced mutations were characterized by statistically significant increases in G → T transversions and small tandem base deletions (16). Drobetsky et al. used a mutation detection system involving adenine phosphoribosyltransferase genes to demonstrate that T→G transversions, which are a generally rare class of mutation, are induced at high frequencies (up to 50%) in UVA-exposed cells (17). These studies indicate that UVA, which constitutes more than 90% of the UV light that reaches the surface of the Earth, is primarily responsible for ROS generation.

On the other hand, recent work has shown that cyclobutane pyrimidine dimers are produced at higher yield than 8-oxoguanine (8-oxoG) after exposure to UVA in

rodent and human skin cells (18–20). We found that the diuretic agent hydrochlorothiazide (HCT) significantly enhanced the production of thymine dimers (T<>Ts) in a wide range of UVA wavelengths, and this enhancement occurred independent of the presence of oxygen (21). This finding indicates that excited HCT molecules function as UVA-absorbing chromophores that transfer energy to adjacent pyrimidines, resulting in the formation of T<>Ts.

UV-INDUCED DNA LESIONS AND MUTATIONS IN SKIN CANCERS

The maximum action spectrum of UV-induced carcinogenesis in animal experiments is within the UVB range, with the peak at 293 nm (22). Direct absorption of UV energy by DNA leads to the formation of pyrimidine photoproducts. Formation of dipyrimidine photoproducts can lead to UV signature mutations, which have been demonstrated in UV irradiated bacteria and mammalian shuttle vectors (23,24). UV signature mutations are known to be a *transition* type mutation, is defined as a change from one pyrimidine (cytosine or thymine) or purine (guanine or adenine) to the other at dipyrimidine sequence site. Many studies have analyzed the molecular changes observed in skin cancers. Ziegler et al. reported that *p53* mutations were detected in nonmelanoma skin cancers from Caucasian people in much higher frequencies, approximately 50 to 90%, than in internal malignancies (6). These mutations are predominated by the C:G → T:A transition type at dipyrimidine sites: namely, the UV signature mutations. Several other reports have demonstrated that the types of mutations that are not considered to be caused by dipyrimidine photoproducts are frequently observed in human skin cancers developed in sun-exposed body sites (25) and UVB-induced murine skin cancer (26), indicating that oxidative DNA damage also plays a role to some extent in cancer development, although dipyrimidine photoproducts remain to be the major players in photocarcinogenesis.

Patients with xeroderma pigmentosum (XP) are deficient in nucleotide excision repair, and their greatly increased susceptibility to skin cancer in sun-exposed areas highlights the role of UV-induced DNA damage in carcinogenesis. XP-A, the most severe type of XP, induces severe photosensitivity, which is obvious within 12 months of age, and the onset of both nonmelanoma skin cancers (NMSCs) and malignant melanomas (MMs) as early as at 10 years of age (21). Most *p53* mutations in skin cancers from XP patients are UV-signature mutations CC → TT base substitutions (27–30). The spectra were similar to those detected in NMSCs of sun-exposed areas of the body in non-XP patients. Comparatively, the frequency of *ras* gene mutations was far less in the same samples. We could detect only one mutation at codon 61 in the Ki-*ras* gene, and the other four mutations found occurred at codons 6, 7, 15, and 16 in the Ha-*ras* gene. The latter mutations are not common and possess a low transforming ability, which implies that DNA damage caused by sunlight rarely affects the crucial sites of the *ras* gene that would lead to the activation of *ras* (31).

A comparative analysis of the mutation frequency and pattern of the *p53* gene in 49 NMSCs, which consisted of 16 basal cell carcinomas (BCCs) and nine

squamous cell carcinomas (SCCs) from sun-exposed areas, and 16 BCCs and eight SCCs from covered areas, indicated that the mutation frequency in the *p53* gene in these two groups were similar at 48% and 46%, respectively. However, the mutational type significantly differed between these two groups; UV signature mutations were detected in 50% (6/12) of tumors that had developed in sun-exposed areas but in less than 20% (2/11) of tumors from covered areas, and this difference was statistically significant (9). This finding indicates that the *p53* mutations detected in the NMSCs that developed in sun-exposed areas are UV signature mutations and that *p53* mutations play a significant role in photocarcinogenesis. These results also suggest that UV light plays a role in inducing mutations in tumor-related genes.

UV-INDUCED INFLAMMATION AND SKIN CANCERS

The most obvious and well-known effect of sun exposure is sunburn (erythema). In humans, slight erythema starts several hours after sun exposure on the site and becomes edematous. Usually, the peak of erythema and swelling is reached 12 to 24 h after exposure and subsides within a few days with pigmentation and, occasionally, fine scales observed. The sunburn reaction depends on several factors, including UV dose, UV wavelength, and skin type. A histological study of moderate doses of UVB irradiation to human skin revealed that dermal neutrophils appeared immediately after irradiation and increased in number from the onset of erythema (0.5 to 4 h) to a maximum at 14 h, dwindling thereafter up to 48 h, thereby indicating that infiltration of neutrophils is a key step in the initiation of acute skin reactions mediated by UVB (32). Following UV absorption by cellular molecules, photochemical reactions occur, and these reactions are responsible for initiating sunburn reactions.

Devary et al. (33) suggested that the UV response is initiated at or near the plasma membrane, and the response may be elicited by oxidative stress caused by UV radiation. Indeed, there is plenty of evidence that various antioxidants attenuate erythema or edema mediated by UVB (34–36). Furthermore, low levels of oxidants can modify cell signaling via redox regulation, and these signal modifications have functional consequences (37). UV irradiation triggers sequential molecular responses, thereby activating cell surface growth factors and pro-inflammatory cytokine receptors. Subsequently, these receptors induce various protein kinase signal transduction pathways that up-regulate expression and functional activation of the nuclear transcription factor AP-1 and thus cause diverse gene expression (38).

Mice treated with the specific p38 mitogen-activated protein kinase (p38 MAPK) inhibitors SB202190 and SB242235 showed marked inhibition of acute sunburn inflammation and apoptosis (39,40). Furthermore, Giri et al. showed that ROS generation followed by the development of cutaneous inflammation after photosensitization acts as a tumor promoter (41). Moore et al. reported that tumor necrosis factor-α (TNF-α)-deficient mice are resistant to skin carcinogenesis (42). They also reported that the frequency of DNA adduct formation and *c-Ha-ras* mutations was the same in wild-type and TNF-$\alpha^{-/-}$ epidermis after 7,12-dimethylbenz[*a*]anthracene (DMBA) treatment. These results imply that this process is independent of initiation.

The pro-inflammatory cytokine TNF-α is a critical mediator of tumor promotion, which acts via the protein kinase C (PKC)-α and AP-1-dependent pathways (43). Persistent oxidative stress in cancer (44) may also cause activation of transcription factors and protooncogenes such as *c-fos* and *c-jun* (45) as well as genetic instability. Such stress may also contribute to the maintenance of malignant characteristics of neoplasms.

We have shown previously that large amounts of 8-OHdG as well as 4-hydroxy-2-nonenal-modified proteins and 3-nitro-L-tyrosine are formed in mice skin after 10 minimal erythema dose (MED) exposures three times per week for 2 weeks (total dose: 100.8 kJ/m^2). In addition, significantly increased 3-nitro-L-tyrosine modifications were detected in the 10 MED-irradiated groups (46); 3-nitro-L-tyrosine suggested the presence of nitric oxide (NO)-mediated oxidative damage in chronic inflammation. Peroxynitrite ($ONOO^-$) is generated by the reaction of NO with superoxide ($O_2^{\bullet -}$), which is released by infiltrating neutrophils and macrophages (47). Immunohistochemical studies of chronically UV-irradiated skin specimens revealed that 8-OHdG is produced not only in the nuclei of epidermal keratinocytes but also in the inflammatory cells. *In vivo* repair kinetics of 8-OHdG demonstrate a slower time to recover to the basal level than for pyrimidine dimers, which suggests an important role of the persistent inflammatory response in oxidative stress (46).

DNA DAMAGE AND INFLAMMATION

We demonstrated previously the high susceptibility to UV-induced skin cancer in *Ogg1* knockout mice, which are deficient in glycosylase/AP lyase, which plays a role in the removal of 8-oxoG from DNA (14). However, unexpectedly, the *p53* mutations found in skin cancers produced in *Ogg1* knockout mice were mainly CC → TT UV signature mutations, not GC → TA transversions, which generally identify the presence of 8-oxoG (48). Furthermore, the gene profiling studies of *Ogg1* knockout mouse skin revealed that the inflammatory response pathway-related genes such as *cxcl1* and *il-6* were the most affected of the up-regulated genes in *Ogg1* knockout mice after UVB exposure (49). In fact, we observed much more neutrophil infiltrate after UV exposure in *Ogg1* knockout mice, indicating that DNA damage (i.e., accumulation of 8-oxoG) caused by the deficiency of the Ogg1 protein leads to mutations. Moreover, the presence of DNA damage itself causes the up-regulation of inflammatory response genes, and it is largely involved in photocarcinogenesis in *Ogg1* knockout mice (14). ROSs caused by direct UV exposure and associated inflammatory reactions caused by UV exposure induce accumulation of oxidative DNA damage, such 8-oxoG in the skin, implying that oxidative DNA damage induced by sunlight plays an important role in the development of skin cancers.

Rodier et al. reported that irreparably large radiation doses induce DNA double-stranded breaks and increase IL-6 secretion (50). We compared *IL-6* levels after 250 mJ/cm^2 of UVB irradiation in wild-type and *Ogg1* knockout mice by real-time PCR (RT-PCR) and found that *Ogg1* knockout mice express significantly higher levels of *IL-6* at 3 and 24 h after UVB exposure than those of wild-type mice. We also performed RT-PCR for inflammatory soluble factors such as *Mmp2* and *Tnfα* but

found no significant difference between the two *Ogg1* genotypes. Our data indicate that IL-1β and IL-6 are the most important candidate cytokines to induce inflammatory conditions associated with 8-oxoG accumulation following UVB exposure.

DIFFERENCE BETWEEN CHEMICALLY INDUCED CANCER AND PHOTOCARCINOGENESIS

Phosphoinositide-specific phospholipase C (PLC), which is an effector of *Ras*, hydrolyzes the membrane phospholipid phosphatidylinositol 4,5-bisphosphate to generate diacylglycerol, which, in turn, activates PKC. *PLCε* knockout ($PLC\varepsilon^{-/-}$) mice exhibit marked resistance to tumor formation in a two-stage skin chemical carcinogenesis protocol using DMBA as an initiator and the phorbol ester 12-*O*-tetradecanoylphorbol-13-acetate (TPA) as a promoter (51). *PLCε* knockout mice also showed reduced inflammatory responses after TPA treatment, suggesting that PLCε positively regulates skin chemical carcinogenesis and the inflammatory response. However, surprisingly, chronic exposure to UVB induced both a greater number and variety of types of skin tumors in $PLC\varepsilon^{-/-}$ mice than in wild-type ($PLC\varepsilon^{+/+}$) and *PLCε* heterozygous ($PLC\varepsilon^{+/-}$) mice (52). Pathophysiological examination revealed that the frequency of UVB-induced cell death in the skin cells of $PLC\varepsilon^{-/-}$ mice was reduced compared with the $PLC\varepsilon^{+/+}$ mice, thereby indicating a crucial role of PLCε in regulating UVB-induced cell death as well as the inflammatory response. It also indicates the importance of UV-induced cell death in the prevention of photocarcinogenesis.

Low levels of oxidants can modify cell-signaling proteins, and these modifications have functional consequences. Gopalakrishna and Jaken demonstrated that various antioxidant preventive agents inhibit PKC-dependent cellular responses and speculated that PKC is a logical candidate for redox modification by oxidants and antioxidants that may determine their cancer-promoting and anticancer activities, respectively (53).

MELANOMA AND UV-INDUCED INFLAMMATION

Recently, much attention has been paid to the occurrence of melanoma formation and UV-induced inflammation. It is generally accepted that continual inflammation increases the risk of cancer, which is consistent with the finding that excessive intense intermittent sun exposure is one of the most important risk factors for melanoma. Noonan et al. reported that a single dose of burning UV radiation to neonates, but not to adults, of the hepatocyte growth factor/scatter factor transgenic mice is necessary and sufficient to induce melanoma with a high incidence (54). This also provides experimental grounds for the epidemiological evidence that childhood sunburn is a major risk factor for the development of melanomas (55,56). Zaidi et al. reported an unanticipated role for interferon-γ (IFN-γ) in promoting melanocytic cell survival/immunoevasion (57). They reported that the expression profile of neonatal skin melanocytes isolated following a melanomagenic UVB dose bear distinct,

persistent interferon response signature, including genes associated with immunoevasion. UVB-induced melanocyte activation, characterized by aberrant growth and migration, was abolished by antibody-mediated systemic blockade of IFN-γ, but not type I interferons. Admixed recruited skin macrophages, which produce IFN-γ, enhanced transplanted melanoma growth; IFN-γ blockade abolished macrophage-enhanced melanoma growth and survival. These findings explain partly why intermittent burning doses of sun exposure is the highest risk factor for melanomagenesis.

Whether UVA or UVB is more dangerous in the development of melanoma is still controversial. Using a fish melanoma model, Setlow et al. reported that UVA is responsible for melanoma development (58), whereas Mitchell et al. reported that UVB, but not UVA, causes melanoma by using a *Xiphophorus* hybrid melanoma model (59). Noonan et al. also reported that UVB, but not UVA, induced melanoma in a mice melanoma model (60). Both NMSCs and melanomas are induced by solar light, but there are some differences. Melanocytes show resistance to UVB-induced apoptosis. Consequently, melanocytes survive after acute sunburn with large amounts of DNA damage, whereas keratinocytes tend to be apoptotic after large doses of UV exposure. These differences explain the discrepancy between chemical carcinogenesis and UV carcinogenesis observed using the PLCε knockout mice. Indeed, the most frequently developed body site of the superficial-spreading type of melanoma, which is the most common type of MM among the Caucasian population, is the trunk or thigh, which is often exposed intensively to the sun when sunbathing. Often, we see sunburn freckles in patients with superficial spreading type MM (SSM). Eumelanin protects the skin from UV, whereas pheomelanin acts as a photosensitizer and causes oxidative DNA damage in melanocytes. Eumelanin predominates in mouse melanocytes, whereas various compositions of eumelanin and pheomelanin are observed in human melanocytes, depending on the skin type. Therefore, careful consideration is necessary when comparing the results in mice with those in humans (61).

THE ROLE OF UVA IN PHOTOCARCINOGENESIS

Until recently, studies on UV-induced carcinogenesis have focused on UVB-induced DNA mutations. However, recently the role of UVA in photocarcinogenesis has received much greater attention. One reason for this is the involvement of UVA-induced ROSs in the development of melanomas. The second reason is that many studies revealed that UVA generates not only ROSs but also cyclobutane pyrimidine dimers *in vivo*. It was demonstrated recently that cyclobutane pyrimidine dimers are produced at higher yields than 8-oxoG after UVA exposure in rodent and human skin cells (18,19); therefore, there was a paradigm shift regarding the theory of photocarcinogenesis. A recent series of studies demonstrating that UVA produces T<>Ts at much higher levels than other types of pyrimidine dimers and does not form 6-4 PPs (20) explains the mutation spectrum of the relevant genes in cancers of sun-exposed areas of the skin in humans (7,27,30). Van Kranen et al. reported that UVA-induced murine skin cancers are less frequent than UVB-induced murine skin cancers and that the incidence of *p53* alterations in UVA-induced tumors is lower than

that in UVB-induced tumors (62). These facts imply that UVB is more mutagenic and carcinogenic than UVA. An *in vivo* study analyzing the action spectrum for photocarcinogenesis in a mice model revealed that UVA is partly responsible for photocarcinogenesis (22). UVA seems to exert cancer-promoting properties besides DNA damage to cause DNA mutations. Many of the carcinogenic functions of UVA have been attributed to its production of ROSs and subsequent induction of the inflammatory signaling pathway. However, it should be noted that UVA is also capable of inducing T<>Ts in human skin.

DEVELOPMENT OF SKIN CANCER IN GENETIC DISORDERS

In mammalian cells, DNA lesions are repaired by several repair systems, such as nucleotide excision repair (NER), base excision repair, and mismatch repair. If the DNA lesions remain at the replication fork, homologous recombination or the translesional DNA synthesis system works. However, if the DNA damage is too extensive to repair via these systems, it may cause mutations. Bulky DNA lesions causing DNA conformational change, such as UV-induced pyrimidine photoproducts, are removed by NER. Deficiency in NER leads to three human genetic diseases: XP, cockayne syndrome (CS), and trichothiodystrophy. Of these, only patients with XP (subdivided into XP-A through XP-G based on the responsible genes) are predisposed to skin cancers. The majority of *p53* mutations in skin cancers from XP patients are CC → TT base substitutions, or UV-signature mutations (27–29). Some investigators have suggested that repair insufficiencies lead to oxidative stress in addition to the accumulation of pyrimidine dimers in XP cells (63,64).

Nevoid basal cell carcinoma syndrome (NBCCS) is an autosomal dominant disease characterized by tumorigenesis, such as multiple BCCs, odontogenic keratocysts, and developmental abnormalities (65). Germline mutations in *PTCH* have been identified in patients with NBCCS (66). In addition, the site-specific distribution of the BCCs in NBCCS patients indicates that UV exposure plays a role in the development of BCCs in NBCCS (67). In the general population, approximately 10% of BCCs occur on the trunk versus 35% among all NBCCS cases. The site-specific distribution of BCCs in Japanese NBCCS indicates a similar tendency (68), suggesting that NBCCS patients are sensitive to intermittent intense sun exposure because people receive occasional intermittent intense sun exposure at this anatomical site. Skin fibroblasts from patients with NBCCS were hypersensitive to death by UVB but not UVC radiation, in comparison with skin fibroblasts from normal individuals; these patients also did not have impaired pyrimidine dimer–removal systems (68,69). A previous report shows that the removal of 8-OHdG in fibroblasts after UVB exposure is slightly impaired in NBCCS cells compared to that in normal cells, which implies that oxidative stress plays a role in the development of BCCs and other tumors in NBCCS (68). Aszterbaum et al. reported that UV and ionizing radiation enhance the growth of BCCs and trichoblastomas in patched heterozygous knockout mice (70).

UV-INDUCED IMMUNE SUPPRESSION

The immune system plays an important role in UV carcinogenesis by contributing to host resistance against skin cancer development. However, UV radiation circumvents immune surveillance against skin cancers by modulating the immune response in a way that favors tumor development. Skin cancers induced by UV radiation are highly antigenic and can therefore be recognized by the immune system. This is apparent with UV-induced murine skin cancers, many of which are immunologically rejected upon transplantation into normal syngenic mice (71). The exceptionally high incidence of skin cancer, particularly squamous cell carcinoma, on the sun-exposed skin of immunosuppressed renal transplant patients (72), suggests that UV-induced human skin cancers are also highly antigenic. However, despite the potential for immunological control, skin cancer occurs with high frequency in susceptible, sun-exposed populations. Previous studies, mainly those using murine models, have provided an explanation for this paradox by demonstrating that UV radiation not only transforms cells by inducing mutations but also interferes with host immunity against the developing skin tumors. These studies demonstrate that UV irradiation of the skin produces both local immune suppression that inhibits immune functions within the irradiated skin and systemic immune suppression against antigens introduced at a critical time after exposure to UV radiation. Modulation of immune responses initiated at nonirradiated sites is now known to involve soluble mediators,

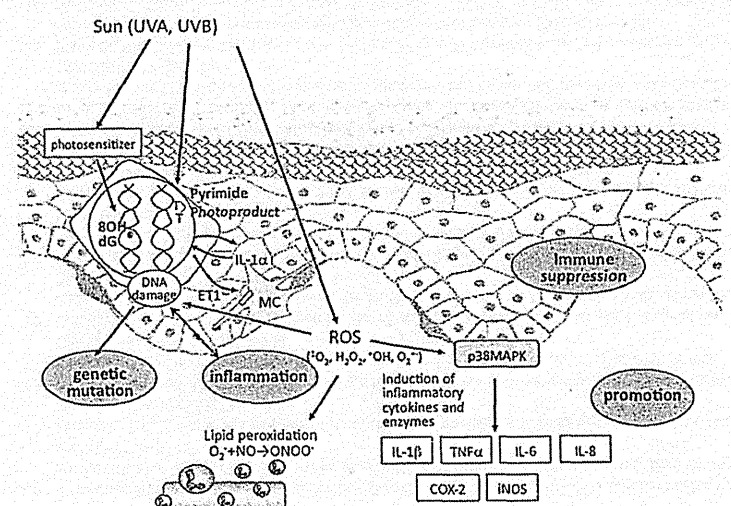

FIGURE 19.1 Schematic summary of photocarcinogenesis detailed in the text. (*See insert for color representation of the figure.*)

at least some of which are produced by UV-irradiated keratinocytes (73). Different mediators appear to be involved in the modulation of delayed-type hypersensitivity (DTH) and the contact hypersensitivity (CHS) response. In particular, IL-10 antibodies prevent UV-induced suppression of DTH responses, whereas TNF-α antibodies inhibit UV-induced suppression of CHS (73). UV-induced pyrimidine dimers have been suggested to trigger cytokine production by epidermal cells, which is involved in UV-induced specific immune suppression (74). Furthermore, lipid peroxidation by UV-induced prostaglandin formation may also play a role in immune suppression (75,76).

In summary, both directly and indirectly, UV induces DNA lesions that cause genetic mutations and trigger inflammation and immune suppression which allow tumor growth. Both UV itself and UV-induced inflammation lead to ROS generation. These ROSs also cause DNA lesions and enhance mutation frequency. Furthermore, lipid peroxidation caused by UV and ROSs is involved in immune suppression (Figure 19.1).

REFERENCES

1. Armstrong BK, Kricker A. The epidemiology of UV induced skin cancer. J Photochem Photobiol B 2001;63:8–18.
2. Hu S, Ma F, Collado-Mesa F, Kirsner RS. UV radiation, latitude, and melanoma in US Hispanics and blacks. Arch Dermatol Res 2004;140:819–824.
3. Das M, Bickers DR, Santella RM, Mukhtar H. Altered patterns of cutaneous xenobiotic metabolism in UVB-induced squamous cell carcinoma in SKH-1 hairless mice. J Invest Dermatol 1985;84: 532–536.
4. Nishigori C, Tanaka M, Moriwaki S, Imamura S, Takebe H. Accelerated appearance of skin tumors in hairless mice by repeated UV irradiation with initial intense exposure and characterization of the tumors. Jpn J Cancer Res 1992;83:1172–1178.
5. Nishigori C, Moriwaki S, Takebe H, Tanaka T, Imamura S. Gene alterations and clinical characteristics of xeroderma pigmentosum group A patients in Japan. Arch Dermatol 1994;130:191–197.
6. Ziegler A, Jonason AS, Leffell DJ, Simon JA, Sharma HW, Kimmelman J, et al. Sunburn and p53 in the onset of skin cancer. Nature 1994;372:773–776.
7. Nishigori C, Hattori Y, Toyokuni S. Role of reactive oxygen species in skin carcinogenesis, Antioxid Redox Signal 2004;6:561–570.
8. Loser K, Apelt J, Voskort M, Mohaupt M, Balkow S, Schwarz T, et al. IL-10 controls ultraviolet-induced carcinogenesis in mice. J Immunol 2007;179:365–371.
9. Nishigori C. Cellular aspects of photocarcinogenesis. Photochem Photobiol Sci 2006;5:208–214.
10. Kvam E, Tyrrell RM. Induction of oxidative DNA base damage in human skin cells by UV and near visible radiation. Carcinogenesis 1997;18:2379–2384.
11. Rosen JE, Prahalad AK, Schlüter G, Chen D, Williams GM. Quinolone antibiotic photodynamic production of 8-oxo-7,8-dihydro-2-deoxyguanosine in cultured liver epithelial cells. Photochem Photobiol 1997;65:990–996.
12. Ellison MJ, Childs JD. Pyrimidine dimers induced in *Escherichia coli* DNA by ultraviolet radiation present in sunlight. Photochem Photobiol 1981;34:465–469.
13. Ono R, Masaki T, Dien S, Yu X, Fukunaga A, Yodoi J, Nishigori C. Suppressive effect of recombinant human thioredoxin on ultraviolet light-induced inflammation and apoptosis in murine skin. J Dermatol 2012;39:843–851.
14. Kunisada M, Sakumi K, Tominaga Y, Budiyanto A, Ueda M, Ichihashi M, et al. 8-Oxoguanine formation induced by chronic ultraviolet B exposure makes *ogg1* knockout mice susceptible to skin carcinogenesis. Cancer Res 2005;65:6006–6010.

15. Ito K, Inoue S, Yamamoto K, Kawanishi S. 8-Hydroxydeoxyguanosine formation at the 5′ site of 5′-GG-3′ sequences in double-stranded DNA by UV radiation with riboflavin. J Biol Chem 1993;268:13221–13227.
16. Besaratinia A, Synold TW, Xi B, Pfeifer GP. G-to-T transversions and small tandem base deletions are the hallmark of mutations induced by ultraviolet A radiation in mammalian cells. Biochemistry 2004;43:8169–8177.
17. Drobetsky EA, Turcotte J, Châteauneuf A. A role for ultraviolet A in solar mutagenesis. Proc Natl Acad Sci USA 1995;92:2350–2354.
18. Douki T, Reynaud-Angelin A, Cadet J, Sage E. Bipyrimidine photoproducts rather than oxidative lesions are the main type of DNA damage involved in the genotoxic effect of solar UVA radiation. Biochemistry 2003;43:9221–9226.
19. Courdavault S, Baudouin C, Charveron M, Favier A, Cadet J, Douki T. Larger yield of cyclobutane dimers than 8-oxo-7,8-dihydroguanine in the DNA of UVA-irradiated human skin cells. Mutat Res 2004;556:135–142.
20. Mouret S, Baudouin C, Charveron M, Favier A, Cadet J, Douki T. Cyclobutane pyrimidine dimers are predominant DNA lesions in whole human skin exposed to UVA radiation. Proc Natl Acad Sci USA 2006;103:13765–13770.
21. Kunisada M, Masaki T, Ono R, Morinaga H, Nakano E, Yogianti F, et al. Hydrochlorothiazide enhances UVA-induced DNA damage. Photochem Photobiol 2013;89:649–654.
22. de Gruijl F. Action spectrum for photocarcinogenesis. Recent Results Cancer Res 1995;139:21–30.
23. Miller J. Mutagenic specificity of ultraviolet light. J Mol Biol 1985;182:45–65.
24. Brash DE, Rudolph JA, Simon JA, Lin A, McKenna GJ, Baden HP, et al. A role for sunlight in skin cancer: UV-induced *p53* mutations in squamous cell carcinoma. Proc Natl Acad Sci USA 1991;88:10124–10128.
25. Pierceall WE, Goldberg LH, Tainsky MA, Mukhopadhyay T, Ananthaswamy HN. *Ras* gene mutation and amplification in human nonmelanoma skin cancers. Mol Carcinog 1991;4:196–202.
26. Nishigori C, Wang S, Miyakoshi J, Sato M, Tsukada T, Yagi T, et al. Mutations in *ras* genes in cells cultured from mouse skin tumors induced by ultraviolet irradiation. Proc Natl Acad Sci USA 1994;91:7189–7193.
27. Dumaz N, Drougard C, Sarasin A, Daya-Grosjean L. Specific UV-induced mutation spectrum in the *p53* gene of skin tumors from DNA-repair-deficient xeroderma pigmentosum patients. Proc Natl Acad Sci USA 1993;90:10529–10533.
28. Sato M, Nishigori C, Zghal M, Yagi T, Takebe H. Ultravioletspecific mutations in *p53* gene in skin tumors in xeroderma pigmentosum patients. Cancer Res 1993;53:2944–2946.
29. Spatz A, Giglia-Mari G, Benhamou S, Sarasin A. Association between DNA repair-deficiency and high level of *p53* mutations in melanoma of xeroderma pigmentosum. Cancer Res 2001;61:2480–2486.
30. Matsumura Y, Sato M, Nishigori C, Zghal M, Yagi T, Imamura S, et al. High prevalence of mutations in the *p53* gene in poorly differentiated squamous cell carcinomas in xeroderma pigmentosum patients. J Invest Dermatol 1995;105:399–401.
31. Sato M, Nishigori C, Lu Y, Zghal M, Yagi T, Takebe H. Far less frequent mutations in *ras* genes than in the *p53* gene in skin tumors of xeroderma pigmentosum patients. Mol Carcinogenesis 1994;11:98–105.
32. Hawk JL, Murphy GM, Holden CA. The presence of neutrophils in human cutaneous ultraviolet-B inflammation. Br J Dermatol 1988;118:27–30.
33. Devary Y, Gottlieb RA, Smeal T, Karin M. The mammalian ultraviolet response is triggered by activation of src tyrosine kinases. Cell 1992;71:1081–1091.
34. Köpcke W, Krutmann J. Protection from sunburn with beta-carotene: a meta-analysis. Photochem Photobiol 2008;84:284–288.
35. Eberlein-König B, Placzek M, Przybilla B. Protective effect against sunburn of combined systemic ascorbic acid (vitamin C) and *d*-alpha-tocopherol (vitamin E). J Am Acad Dermatol 1998;38:45–48.
36. Katiyar SK, Perez A, Mukhtar H. Green tea polyphenol treatment to human skin prevents formation of ultraviolet light B–induced pyrimidine dimers in DNA. Clin Cancer Res 2000;6:3864–3869.
37. Sun Y, Oberley LW. Redox regulation of transcriptional activators. Free Radic Biol Med 1996;21:335–348.
38. Rittié L, Fisher GJ. UV-light-induced signal cascades and skin aging. Ageing Res Rev 2002;1: 705–720.

39. Hildesheim J, Rania TA, Fornace AJ. p38 Mitogen-activated protein kinase inhibitor protects the epidermis against the acute damaging effects of ultraviolet irradiation by blocking apoptosis and inflammatory responses. J Invest Dermatol 2004;122:497–502.
40. Kim AL, Labasi JM, Zhu Y, Tang X, McClure K, Gabel CA, et al. Role of p38 MAPK in UVB-induced inflammatory responses in the skin of SKH-1 hairless mice. J Invest Dermatol 2005;124: 1318–1325.
41. Giri U, Sharma SD, Abdulla M, Athar M. Evidence that *in situ* generated reactive oxygen species act as a potent stage I tumor promoter in mouse skin. Biochem Biophys Res Commun 1995;209:698–705.
42. Moore RJ, Owens DM, Stamp G, Arnott C, Burke F, East N, et al. Mice deficient in tumor necrosis factor-alpha are resistant to skin carcinogenesis. Nat Med 1999;5:828–831.
43. Arnott CH, Scott KA, Moore RJ, Hewer A, Phillips DH, Parker P, et al. Tumour necrosis factor-alpha mediates tumour promotion via a PKC alpha- and AP-1-dependent pathway. Oncogene 2002;21:4728–4738.
44. Toyokuni S, Okamoto K, Yodoi J, Hiai H. Persistent oxidative stress in cancer. FEBS Lett 1995;358:1–3.
45. Crawford D, Zbinden I, Amstad P, Cerutti P. Oxidant stress induces the proto-oncogenes c-*fos* and c-*myc* in mouse epidermal cells, Oncogene 1988;3:27–32.
46. Hattori Y, Nishigori C, Tanaka T, Uchida K, Nikaido O, Osawa T, et al. 8-Hydroxy-2′-deoxyguanosine is increased in epidermal cells of hairless mice after chronic ultraviolet B exposure. J Invest Dermatol 1996;107:733–737.
47. Kaur H, Halliwell B. Evidence for nitric oxide–mediated oxidative damage in chronic inflammation: nitrotyrosine in serum and synovial fluid from rheumatoid patients. FEBS Lett 1994;350:9–12.
48. Yogianti F, Kunisada M, Ono R, Sakumi K, Nakabeppu Y, Nishigori C. Skin tumours induced by narrowband UVB have higher frequency of *p53* mutations than tumours induced by broadband UVB independent of *Ogg1* genotype. Mutagenesis 2012;27:637–643.
49. Kunisada M, Yogianti F, Sakumi K, Ono R, Nakabeppu Y, Nishigori C. Increased expression of versican in the inflammatory response to UVB- and reactive oxygen species–induced skin tumorigenesis. Am J Pathol 2011;179:3056–3065.
50. Rodier F, Coppé JP, Patil CK, Hoeijmakers WA, Muñoz DP, Raza SR, et al. Persistent DNA damage signalling triggers senescence-associated inflammatory cytokine secretion. Nat Cell Biol 2009;11:973–979.
51. Bai Y, Edamatsu H, Maeda S, Saito H, Suzuki N, Satoh T, et al. Crucial role of phospholipase Cepsilon in chemical carcinogen-induced skin tumor development. Cancer Res 2004;64:8808–8810.
52. Oka M, Edamatsu H, Kunisada M, Hu L, Takenaka N, Dien S, et al. Enhancement of ultraviolet B–induced skin tumor development in phospholipase Ce-knockout mice is associated with decreased cell death. Carcinogenesis 2010;31:1897–1902.
53. Gopalakrishna R, Jaken S. Protein kinase C signaling and oxidative stress. Free Radic Biol Med 2000;28:1349–1361.
54. Noonan FP, Recio JA, Takayama H, Duray P, Anver MR, Rush WL, et al. Neonatal sunburn and melanoma in mice. Nature 2001;413:271–272.
55. Autier P, Doré JF. Influence of sun exposures during childhood and during adulthood on melanoma risk. EPIMEL and EORTC Melanoma Cooperative Group. European Organisation for Research and Treatment of Cancer. Int J Cancer 1998;77:533–537.
56. Whiteman DC, Whiteman CA, Green AC. Childhood sun exposure as a risk factor for melanoma: a systematic review of epidemiologic studies. Cancer Causes Control 2001;12:69–82.
57. Zaidi MR, Davis S, Noonan FP, Graff-Cherry C, Hawley TS, Walker RL, et al. Interferon-γ links ultraviolet radiation to melanomagenesis in mice. Nature 2011;469:548–553.
58. Setlow RB, Grist E, Thompson K, Woodhead AD. Wavelengths effective in induction of malignant melanoma. Proc Natl Acad Sci USA 1993;90:6666–6670.
59. Mitchell DL, Fernandez AA, Nairn RS, Garcia R, Paniker L, Trono D, et al. Ultraviolet A does not induce melanomas in a *Xiphophorus* hybrid fish model. Proc Natl Acad Sci USA 2010;107:9329–9334.
60. Noonan FP, Zaidi MR, Wolnicka-Glubisz A, Anver MR, Bahn J, Wielgus A, et al. Melanoma induction by ultraviolet A but not ultraviolet B radiation requires melanin pigment. Nat Commun 2012;3:884.
61. Hill HZ, Hill GJ. UVA, pheomelanin and the carcinogenesis of melanoma. Pigment Cell Res 2000;13 Suppl 8:140–144.

62. van Kranen HJ, de Laat A, van de Ven J, Wester PW, de Vries A, Berg RJ, et al. Low incidence of p53 mutations in UVA (365-nm)-induced skin tumors in hairless mice. Cancer Res 1997;57:1238–1240.
63. Reardon JT, Bessho T, Kung HC, Bolton PH, Sancar A. *In vitro* repair of oxidative DNA damage by human nucleotide excision repair system: possible explanation for neurodegeneration in xeroderma pigmentosum patients. Proc Natl Acad Sci USA 1997;94:9463–9468.
64. Satoh MS, Jones CJ, Wood RD, Lindahl T. DNA excision-repair defect of xeroderma pigmentosum prevents removal of a class of oxygen free radical–induced base lesions. Proc Natl Acad Sci USA 1993;90:6335–6339.
65. Gorlin RJ. Nevoid basal-cell carcinoma syndrome. Medicine (Baltim) 1987;66:98–113.
66. Hahn H, Wicking C, Zaphiropoulous PG, Gailani MR, Shanley S, Chidambaram A, et al. Mutations of the human homolog of *Drosophila* patched in the nevoid basal cell carcinoma syndrome. Cell 1996;85:841–851.
67. Goldstein AM, Bale SJ, Peck GL, DiGiovanna JJ. Sun exposure and basal cell carcinomas in the nevoid basal cell carcinoma syndrome. J Am Acad Dermatol 1993;29:34–41.
68. Nishigori C, Arima Y, Matsumura Y, Matsui M, Miyachi Y. Impaired removal of 8-hydroxydeoxyguanosine induced by UVB radiation in naevoid basal cell carcinoma syndrome cells. Br J Dermatol 2005;153 (Suppl 2):52–56.
69. Applegate LA, Goldberg LH, Ley RD, Ananthaswamy HN. Hypersensitivity of skin fibroblasts from basal cell nevus syndrome patients to killing by ultraviolet B but not by ultraviolet C radiation. Cancer Res 1990;50:637–641.
70. Aszterbaum M, Epstein J, Oro A, Douglas V, LeBoit PE, Scott MP, et al. Ultraviolet and ionizing radiation enhance the growth of BCCs and trichoblastomas in patched heterozygous knockout mice. Nat Med 1999;5:1285–1291.
71. Kripke ML. Antigenicity of murine skin tumors induced by ultraviolet light. J Natl Cancer Inst 1974;53:1333–1336.
72. Glover MT, Niranjan N, Kwan JT, Leigh IM. Non-melanoma skin cancer in renal transplant recipients: the extent of the problem and a strategy for management. Br J Plast Surg 1994;47:86–89.
73. Rivas JM, Ullrich SE. The role of IL-4, IL-10, and TNF-α in the immune suppression induced by ultraviolet radiation. J Leukocyte Biol 1994;56:769–775.
74. Nishigori C, Yarosh DB, Ullrich SE, Vink AA, Bucana CD, Roza L, et al. Evidence that DNA damage triggers interleukin 10 cytokine production in UV-irradiated murine keratinocytes. Proc Natl Acad Sci USA 1996;93:10354–10359.
75. Shreedhar V, Giese T, Sung VW, Ullrich SE. A cytokine cascade including prostaglandin E2, IL-4, and IL-10 is responsible for UV-induced systemic immune suppression. J Immunol 1998;160:3783–3789.
76. Halliday GM. Inflammation, gene mutation and photoimmunosuppression in response to UVR-induced oxidative damage contributes to photocarcinogenesis. Mutat Res 2005;571:107–120.

ORIGINAL ARTICLE

Inhibitory Effects of Dietary *Spirulina platensis* on UVB-Induced Skin Inflammatory Responses and Carcinogenesis

Flandiana Yogianti[1,2], Makoto Kunisada[1], Eiji Nakano[1], Ryusuke Ono[1], Kunihiko Sakumi[3], Sugako Oka[3], Yusaku Nakabeppu[3] and Chikako Nishigori[1]

Reactive oxygen species produced in response to UVR are important in skin tumor development. We have previously reported that deficiency of the *Ogg1* gene, encoding the repair enzyme for 8-oxo-7,8-dihydroguanine (8-oxoG), increases skin tumor incidence in mice upon repetitive UVB exposure and modulation of UVB-induced inflammatory response. *Spirulina platensis* is used as a human food supplement because it contains abundant nutritional and antioxidant components. Therefore, we investigated the inhibitory effects of *S. platensis* on UVB-induced skin tumor development in *Ogg1* knockout-(KO) mice and the wild-type (WT) counterpart. Dietary *S. platensis* suppressed tumor induction and development in both genotypes compared with our previous data without *S. platensis*. Induction of erythema and ear swelling, one of the hallmarks of UVB-induced inflammatory responses, was suppressed in the skin of *Ogg1*-KO mice and albino hairless mice fed with dietary *S. platensis*. Compared with untreated mice, *S. platensis*-administered mice showed significantly reduced 8-oxoG formation in the skin after UVB exposure. Moreover, we found that *S. platensis* effectively downregulated the signal proteins p38 mitogen-activated protein kinase, stress-activated protein kinase/c-Jun N-terminal kinase, and extracellular signal–regulated kinase after UVB exposure especially in *Ogg1*-KO mice. Our results suggest that *S. platensis* exerts antitumor effects against UVB irradiation in the skin through its anti-inflammatory and antioxidant effects.

Journal of Investigative Dermatology (2014) **134,** 2610–2619; doi:10.1038/jid.2014.188; published online 29 May 2014

INTRODUCTION

UV light is a carcinogenic component of sunlight and is widely known as one of the most relevant risk factors for skin cancers (Slaper *et al.*, 1996; Urbach, 1997; Howe *et al.*, 2001). Irradiation of mouse skin with UVB (wavelength, 280–320 nm) causes various photochemical reactions, such as induction of DNA damage and the subsequent gene mutation, which may lead to skin cancer development (Nishigori, 2006). Previous studies have demonstrated that UVB induces the formation of 8-oxo-7,8-dihydroguanine (8-oxoG) in mice through UVB-induced reactive oxygen species (ROS; Hattori *et al.*, 1996; Nishigori *et al.*, 2004). The *Ogg1* gene encodes a repair enzyme that removes the oxidized base 8-oxoG-DNA from DNA (Maki and Sekiguchi, 1992; Aburatani *et al.*, 1997; Nakabeppu *et al.*, 2010). In a previous series of studies, *Ogg1*-KO mice showed increasing frequency of mutations but did not exhibit cancer-prone phenotypes in livers and testes (Klungland *et al.*, 1999; Minowa *et al.*, 2000). On the other hand, Sakumi *et al.* demonstrated an increase in the rate of spontaneous lung cancer development in *Ogg1*-KO mice (Sakumi *et al.*, 2003). In our previous study, we found that *Ogg1*-KO mice had a highly tumorigenic phenotype, more numerous skin cancers, and much faster tumor development upon repetitive UVB exposure compared with WT mice (Kunisada *et al.*, 2005).

Spirulina platensis (*S. platensis*) is a blue-green filamentous alga that is currently gaining increasing attention because of its nutritional benefits. Recently, *S. platensis* has been reported to have potential roles in the inhibition of the NADPH oxidase activity (McCarty *et al.*, 2010; Zheng *et al.*, 2013). Owing to its high content of proteins (60–70%) and vitamins (e.g., vitamin B_{12} and provitamin A (β-carotene)), minerals (e.g., iron), and essential fatty acids (e.g., γ-linolenic acid),

[1]*Division of Dermatology, Department of Internal Related, Graduate School of Medicine, Kobe University, Kobe, Japan;* [2]*Department of Dermatology and Venereology, Faculty of Medicine, Gadjah Mada University, Yogyakarta, Indonesia and* [3]*Division of Neurofunctional Genomics, Medical Institute of Bioregulation, Kyusyu University, Fukuoka, Japan*

Correspondence: Chikako Nishigori, Division of Dermatology, Department of Internal Related, Graduate School of Medicine, Kobe University, Kobe 650-0017, Japan. E-mail: chikako@med.kobe-u.ac.jp

Abbreviations: ERK, extracellular signal–regulated kinase; IL, interleukin; KO, knockout; MEFs, mouse embryonic fibroblasts; PCB, phycocyanobilin; p38 MAPK, p38 mitogen-activated protein kinase; ROS, reactive oxygen species; SAPK/JNK, stress-activated protein kinase/c-Jun N-terminal kinase; TLR, Toll-like receptor; WT, wild-type; 8-oxoG, 8-oxo-7,8-dihydroguanine

Received 21 November 2013; revised 7 March 2014; accepted 17 March 2014; accepted article preview online 14 April 2014; published online 29 May 2014

S. platensis has been produced widely as a food supplement (Belay *et al.*, 1993). Several previous toxicity studies showed that there were no adverse effects in experimental animals after short-term and long-term ingestion of dietary *Spirulina (S. platensis* and *Spirulina maxima*), even after administration of high doses (Salazar *et al.*, 1998; Hutadilok-Towatana *et al.*, 2008). In addition, *S. platensis* has been reported to have various beneficial effects, such as anticancer (Dasgupta *et al.*, 2001; Ismail *et al.*, 2009; Grawish *et al.*, 2010), hepatoprotective (Ismail *et al.*, 2009; Lu *et al.*, 2010), antiviral (Hayashi *et al.*, 1996a, b), anti-allergic (Kim *et al.*, 1998), cardioprotective (Khan *et al.*, 2005), and neuroprotective effects (Bermejo-Bescos *et al.*, 2008). However, the effects of *S. platensis* on UVB-induced responses in the skin still remain unclear. In the present study, we investigated whether dietary *S. platensis* affects skin tumor development in *Ogg1* knockout (KO)-mice induced by long-term UVB exposure and demonstrated its inhibitory effects. Furthermore, we examined whether *S. platensis* suppressed the inflammatory response caused by UVB as we had earlier found that the genes involved in inflammatory responses were mostly upregulated by UVB in *Ogg1*-KO mice, which are susceptible to photocarcinogenesis.

RESULTS

Dietary *S. platensis* inhibited the development and induction of UVB-induced skin tumors

We compared the development of skin tumors induced by chronic exposure to the minimum erythema dose of UVB in *Ogg1*-KO and WT mice fed *S. platensis* (SP(+)) or those not fed *S. platensis* (SP(−)). The total number of skin tumors that developed was significantly higher in the groups of SP(−) mice than those in SP(+); (WT, $P<0.01$; KO, $P<0.00001$). The ratios of malignant tumors/total tumors were not significantly different between SP(−) and SP(+) groups in both genotype mice (Table 1). Histological analysis of all the skin tumors showed that the ratios of malignant tumors were 50 and 66.7% in WT and *Ogg1*-KO mice, respectively, among the skin tumors that developed in the SP(+) group. In the case of the SP(−) group, the ratios of malignant tumors were 50 and 88.5% in WT and *Ogg1*-KO mice, respectively (Table 1). Next, we examined skin tumor induction by chronic UVB exposure in the SP(−) and SP(+) groups, and in each *Ogg1* genotype. As shown in Figure 1, in *Ogg1*-KO mice, the first incidence of skin tumor in SP(−) group was 7 weeks earlier than that in SP(+). After 41 weeks, 100% of *Ogg1*-KO/SP(−) mice harbored skin tumors. In the SP(+) group, by the end of the experiment, we found skin tumors in only 40% of the total population. A similar pattern was observed in the WT mice; the first skin tumor was found during week 37 of the experiment in the WT/ SP(+) group, which is 1 week later than in the WT/SP(−) group. At week 44, only 37.5% of all the WT/SP(+) mice were found to harbor skin tumors, whereas 100% of the WT/SP(−) mice showed tumors (Figure 1). In both genotypes, the incidence of UVB-induced skin tumors was significantly different in these two diet groups. However, in the case of the SP(+) group, there was no significant difference in tumor induction between the different

Table 1. Skin tumor formation by chronic UVB irradiation for each *Ogg1* genotype with or without supplementation of 10% *Spirulina platensis* diet

Ogg1 genotype	*Spirulina platensis* diet	Total number of tumors			Mean number of tumors per mouse	Histological analysis, %					
						Malignant tumors, %				Benign tumor	
		Male	Female	Total		Squamous cell carcinoma	Sarcoma	Total	Papilloma	Unidentified[a]
WT	(+)	2 (2)[b]	2 (6)	4 (8)	0.5 ± 0.76*	50.0 (2/4)[c]	0 (0/4)	50[d] (2/4)	50 (2/4)	0 (0/4)
	(−)	2 (1)	10 (6)	12 (7)	1.71 ± 0.76*	41.7 (5/12)	8.3 (1/12)	50[d] (6/12)	41.7 (5/12)	8.3 (1/12)
KO	(+)	0 (2)	6 (8)	6 (10)	0.6 ± 0.84**	50.0 (3/6)	16.7 (1/6)	66.7[d] (4/6)	16.7 (1/6)	16.7 (1/6)
	(−)	5 (1)	21 (6)	26 (7)	3.71 ± 1.38**	73.1 (19/26)	15.4 (4/26)	88.5[d] (23/26)	11.5 (3/26)	0 (0/26)

Abbreviations: KO, knockout; WT, wild-type.
[a]Unidentified tumors for which we were not able to make the diagnosis due to the failure of the procedure of embedding the specimens.
[b]The number of skin tumor–bearing mice at the end of experiment.
[c]The number of skin tumors/total skin tumors histologically.
[d]Not significant.
*$P<0.01$, **$P<0.0001$. There were 10 mice in each group at the beginning of the experiment; during the experiment some mice died and those were not included.
Data from our previous study for the SP (−) group of WT and *Ogg1*-KO mice were used. (Kunisada *et al.*, 2005).

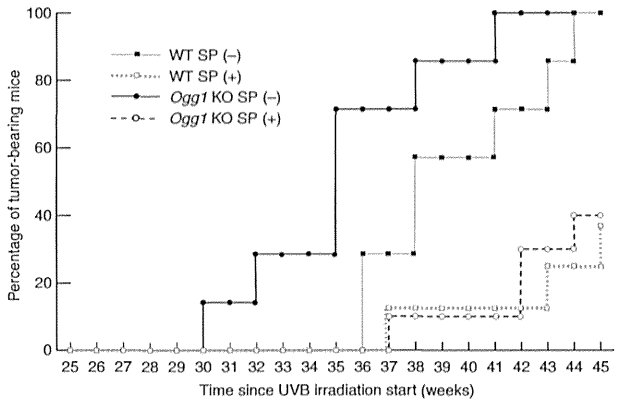

Figure 1. Differences in tumor induction by repetitive UVB irradiations in *Ogg1*-KO and WT mice with or without the *Spirulina platensis* (SP) diet. Each group was composed of 10 mice at the beginning of the experiment. After 40 weeks of chronic UVB exposure, we continued the observation to evaluate tumor development for another 5 weeks. The data for WT/SP(−) and KO/SP(−) mice have been obtained from our previously published study (Kunisada *et al.*, 2005). KO, knockout; WT, wild-type.

Ogg1 genotypes (Figure 1). The data for the SP(−) group of WT mice and *Ogg1*-KO mice have been reproduced here from the results of our previous study (Kunisada *et al.*, 2005). The duration of the experiment and UV irradiation protocols were the same in the present and previous studies and one of the experimenters was involved in both studies. The procedure for chow production was the same with or without *S. platensis*, and was carried out by the same company.

Oral dietary *S. platensis* suppressed UVB-induced ear swelling and skin erythema

We had previously reported that the most upregulated genes in *Ogg1*-KO mice after UVB irradiation were those involved in the inflammatory response, suggesting that the immunomodulation seen after UVB irradiation in *Ogg1*-KO mice might have a role in its highly skin tumor–prone *Ogg1*-KO phenotype (Kunisada *et al.*, 2011). To evaluate the inflammatory response in the skin of mice belonging to the SP(−) or SP(+) group, ear swelling was assessed over a 6-day-period after 4 weeks of oral administration of 10% *S. platensis* followed by a single irradiation of 2.50 kJ m^{-2} UVB to *Ogg1*-KO and WT mice. The peak value for ear swelling was obtained 96 hours after UVB irradiation in all the groups, and significant differences were observed at every time point between SP(−) and SP(+) of each *Ogg1* genotype (WT: $P=0.018$; KO: $P=0.019$; Figure 2a). Next, we studied whether the similar response could be observed in another mouse strain. We applied a protocol similar to that used for *Ogg1*-KO and WT mice to hairless albino mice, except for the UV dose, and then evaluated the erythema scores as well as ear swelling as an inflammatory response upon UVB exposure. A similar inhibitory effect on ear swelling was observed by *S. platensis* in the hairless albino mice: the SP(+) group showed significantly less ear swelling at every time point compared with the SP(−) group after UVB exposure ($P=0.012$; Figure 2b). The erythema on the back skin of hairless albino mice peaked at 72 hours after UVB exposure in both diet groups, with the SP(+) mice showing a much lower degree of erythema and lower amount of scales than the mice belonging to the SP(−) group (Figure 2c). When we scored the degree of erythema, the difference between the SP(−) and SP(+) groups was statistically significant after UVB irradiation ($P=0.011$; Figure 2d).

UVB-induced inflammatory cytokines and Toll-like receptor 4 were attenuated in the skin of *Ogg1*-KO mice fed with *S. platensis*

We had previously reported that IL1-β as well as Cxcl1 is the most important cytokine candidate in the induction of inflammation associated with 8-oxoG accumulation after UVB exposure (Kunisada *et al.*, 2011 and unpublished data). We examined the expression of *IL1-β* and *Cxcl1* after UVB exposure in *Ogg1*-KO and WT mice from the SP(−) and SP(+) groups by using quantitative PCR (qPCR). The difference in interleukin (*IL-1β*) expression between the SP(−) and SP(+) groups in either genotype was most prominent at 24 hours after UVB irradiation. *S. platensis* showed significant inhibition of *IL-1β* expression at all the time points in *Ogg1*-KO mice and at 24 hours after UVB exposure in WT mice ($P<0.05$; Figure 3a). qPCR showed that SP significantly inhibited *Cxcl1* expression at 24 hours after UVB irradiation in *Ogg1*-KO mice and at 6 hours after UVB irradiation in WT mice ($P<0.05$). There was no difference in the expression of *Cxcl1* between the two diet groups for either genotype of mice at other time points (Figure 3b). To confirm the results obtained for *IL1-β* with qPCR, we performed an immunohistochemical study for IL1-β expression in the skin of mice belonging to the SP(−) and SP(+) groups. The epidermal cell expression of IL1-β clearly increased in the *Ogg1*-KO genotype for SP(−) at 24 hours after exposure (Figure 3c). Recently, Toll-like receptor 4 (TLR4) was found to be associated with skin tumorigenesis, via induction of production of proinflammatory cytokines such as IL1-β, IL-6, and tumor necrosis factor-α (Mittal *et al.*, 2010). Our immunohistochemical study showed that TLR4 expression 24 hours after UVB exposure was attenuated in the epidermal cells as well as the dermal inflammatory cells in the SP-treated group in both genotype mice. The attenuation was much more striking in *Ogg1*-KO mice than in WT mice (Figure 3d and e).

Reduction of oxidatively damaged DNA in *S. platensis*–treated mice

We investigated the relevance of UVB-induced formation of epidermal DNA damage such as 8-oxoG and CPDs among the SP(+) and SP(−) groups at 3 and 24 hours after UVB exposure. *Ogg1*-KO/SP(−) mice showed the highest accumulation of 8-oxoG at 3 hours, and even at 24 hours, after UVB exposure. WT mice showed minimal accumulation of 8-oxoG at 3 hours after irradiation, and these levels had decreased almost to zero 24 hours after UVB irradiation. In contrast, both genotypes of the SP(+) group showed less accumulation of 8-oxoG at 3 and 24 hours after UVB exposure (Figure 4a).

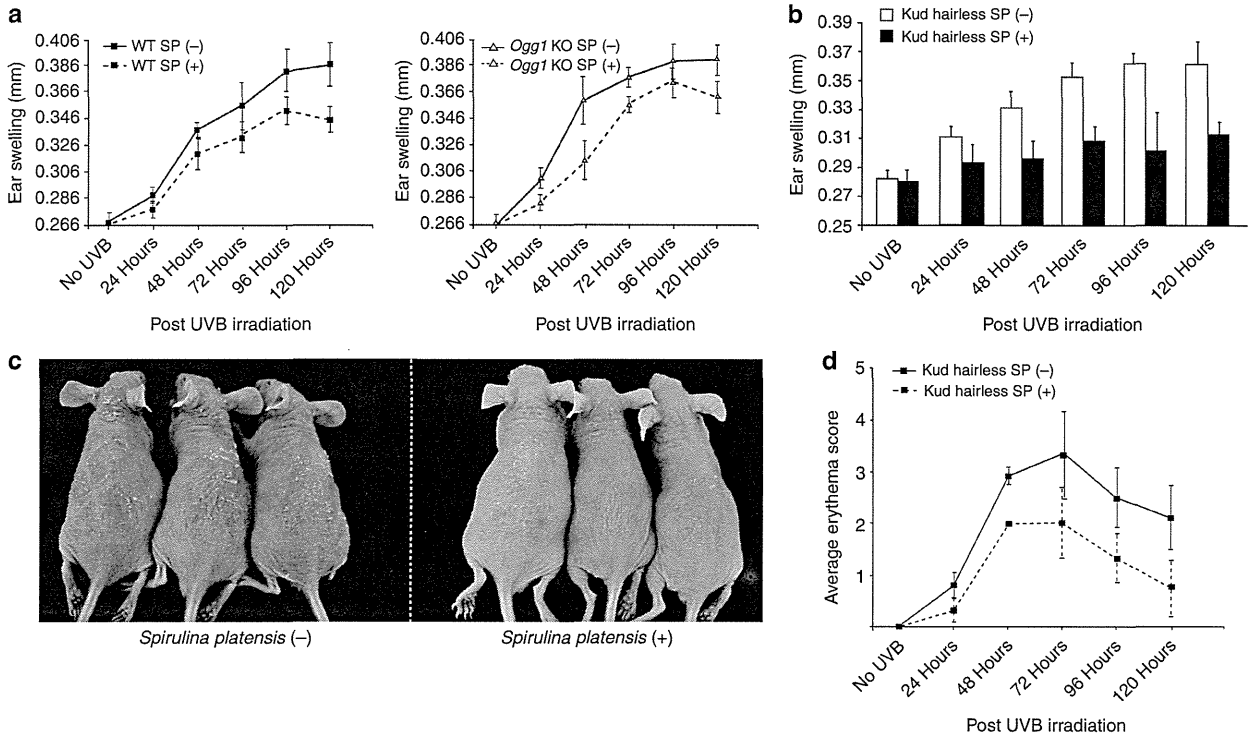

Figure 2. The acute inflammatory response mediated by UVB exposure in mouse skin was attenuated by supplementation with the 10% *Spirulina platensis* (SP) diet. (**a**) After 4 weeks of oral administration of 10% *S. platensis* followed by single irradiation of 2.50 kJ m^{-2} UVB to *Ogg1*-KO and WT mice, ear thickness was measured at 24, 48, 72, 96, and 120 hours after UVB irradiation as well as before UVB treatment. Evaluation of ear thickness was visualized with graphs for WT/SP(−) and WT/SP(+) (left) and for KO/SP(−) and KO/SP(+) (right) mice. Values shown are mean ± SD (**b**) Ear thickness was evaluated using Kud hairless mice given SP(−) and SP(+) diets. The protocol for the hairless mice was identical to that for *Ogg1*-KO and WT mice, except that the UVB dose was 1.50 kJ m^{-2}. Values shown are mean ± SD. (**c**) Erythema induction on the back skin of hairless mice under both SP(−) and SP(+) diets induced by UVB exposure. Before UVB irradiation, hairless mice were fed 10% *S. platensis*. Representative features of the back skin at 72 hours after UVB irradiation in three mice from the SP(−) group (left) and in three mice from the SP(+) group (right), respectively, are shown. (**d**) The average erythema score was measured for the back skin of hairless mice without UVB or at 24, 48, 72, 96, and 120 hours after UVB irradiation. Values shown are mean ± SD. KO, knockout; WT, wild-type.

To confirm whether the UVB dose used for each group was sufficient to cause DNA damage, we performed immunohistochemical analysis of CPDs, showing strongly CPD-positive cells regardless of the ingestion of the *S. platensis* diet or the *Ogg1* genotype (Figure 4b).

Phosphorylation of the stress-activated protein kinases, p38 MAPK, SAPK/JNK, and ERK, was suppressed by *S. platensis*

Furthermore, to investigate the molecular mechanism underlying the suppressive effect of *S. platensis* on the acute inflammatory response mediated by UVB, we examined phosphorylation in the p38 mitogen-activated protein kinase (p38 MAPK), stress-activated protein kinase/c-Jun N-terminal kinase (SAPK/JNK), and extracellular signal–regulated kinase (ERK) pathways after a single irradiation with UVB and studied the protein levels at various time points in either *Ogg1*-KO or WT mice from the SP(−) and SP(+) groups by using immunohistochemistry analysis. In WT mice, p38 MAPK phosphorylation and phosphorylation of SAPK/JNK was suppressed at 30 minutes after UVB exposure in the SP(+) group (Figure 5a and b), whereas no obvious differences were observed in the expression of phosphorylated ERK between SP(−) and SP(+) mice at any time point (Figure 5c). In contrast, for *Ogg1*-KO mice, the phosphorylation of p38 MAPK, SAPK/JNK, and ERK was inhibited to a greater extent in SP(+) than in SP(−) mice at every time point after UVB irradiation (Figure 5a–c). Finally, we used *Ogg1*$^{(+/+)}$ and *Ogg1*$^{(-/-)}$ mouse embryonic fibroblasts (MEFs); phycocyanobilin, active form of main functioning protein C-phycocyanin in *S. platensis*, covalently attached to the apoprotein (Figure 5d) was used for specifically analyzing the signal protein kinases after UVB exposure (Schram and Kroes, 1971). In *Ogg1*$^{(+/+)}$ MEFs, no obvious differences were observed in the expression of phosphorylated p38 MAPK between PCB(−) and PCB(+) mice at any time point, whereas phosphorylation of SAPK/JNK and ERK was suppressed at 2 and 6 hours after UVB exposure in the PCB(+) group in *Ogg1*$^{(+/+)}$ (Figure 5e). In contrast, for *Ogg1*$^{(-/-)}$, the phosphorylation of p38 MAPK was inhibited to a greater extent by PCB(+) at 30 minutes after UVB irradiation. SAPK/JNK phosphorylation was also suppressed by PCB(+) in *Ogg1*$^{(-/-)}$at every time point after UVB exposure (Figure 5f). Moreover, at later time points (e.g., 6 and 24 hours), ERK phosphorylation was significantly suppressed in the *Ogg1*$^{(-/-)}$/PCB(+) group (Figure 5f).